UNIVERSITY OF CALIFORNIA, SAN DIEGO

# Statistical analysis of solar irradiation in a distributed microgrid

A Thesis submitted in partial satisfaction of the requirements
for the degree Master of Science

in

Engineering Sciences (Mechanical Engineering)

by

James Patrick Harper

Committee in charge:

Professor Jan Kleissl, Chair
Professor Ery Arias-Castro
Professor Anne Hoger

2010

The Thesis of James Patrick Harper is approved and it is acceptable in quality and form for publication on microfilm and electronically:

_____

_____

_____

Chair

University of California, San Diego

2010

# DEDICATION

For Jim Davin, for inspiring me to become an engineer;

For my parents, in recognition of the many years of their unwavering support, confidence in my abilities and love;

And for Star Trek, for providing a hopeful picture of our future world, made possible by embracing new ideas and technologies.

# EPIGRAPH

“If sunbeams were weapons of war, we would have had solar energy centuries ago.”

— Sir George Porter

# TABLE OF CONTENTS

# LIST OF ABBREVIATIONS

| | |
|---|---|
| GHI | global horizontal irradiation |
| SKC | sky clear |
| PV | photovoltaic |
| DifSI | diffuse solar irradiation |
| DirSI | direct solar irradiation |
| PDF | probability density function |
| SS | step size |
| RR | ramp rate |

# LIST OF FIGURES

# LIST OF TABLES

# ACKNOWLEDGEMENTS

I would like to thank Professor Jan Kleissl for his support as the chair of my committee. His excellent guidance, constant availability and expertise have proven to be invaluable over the past year.

I would also like to acknowledge Stephen Wilcox and David Renné of the National Renewable Energy Laboratory in Golden, CO for their expert advice in helping to determine the path of this project and for the use of their program “Sunny Days.”

ABSTRACT OF THE THESIS

# Statistical analysis of solar irradiation in a distributed microgrid

by

James Patrick Harper

Master of Science in Engineering Sciences (Mechanical Engineering)

University of California, San Diego, 2010

Professor Jan Kleissl, Chair

In recent decades, solar power has become increasingly more efficient and wide-spread in its use, particularly in residential applications. To allow residential solar power to continue its growth and become a larger percentage of energy production in the United States, the issues of solar intermittency must be understood. This project builds upon previous research in this field by analyzing 1-second solar irradiation data gathered over 5 months by a unique array of 8 sites around the campus of UC San Diego. Correlations between the sites in both time and space, stratification of days by cloudiness, and ramp rate analysis are used to examine the variability of the solar power produced at the sites, while an aggregate ramp rate analysis is used to draw conclusions about the character of the net power produced from a distributed array of solar sites. These analyses have shown important characteristics of residential solar power generation that were previously not well described in the literature.

# 1. INTRODUCTION

Over the past few decades, solar power has become increasingly more efficient and wide-spread in its use. In fact, installed peak solar power capacity has increased nearly exponentially since 1980 to the present day figure of 225 $GW_p$/year, of which 100 GWp/year is grid-connected (1). However, this figure pales in comparison to the 6.93 PWh/year production of power from coal in the United States alone (2).

To allow solar power to continue its growth and become a larger percentage of energy production in the United States, the issue of solar intermittency must be addressed. Intermittency in solar power is caused by both cyclic (diurnal and seasonal) fluctuations, as well as non-cyclic weather phenomena, and can result in difficulties when powering a constant load (3). However, understanding the characteristics of these intermittencies can help mitigating their effects.

Long and Ackerman 1994 investigated the spatial correlation of global horizontal solar irradiation (GHI) between sites separated by between 10 and 90 km (4). They discovered that daily variation was large between sites, mainly due to cloud cover type. Their research also confirmed that correlation between sites decreased rapidly as the distance between the sites was increased, as was expected.

Long and Ackerman also showed that by removing the diurnal cycle via subtracting a model clear-sky (SKC) profile of GHI from measured GHI, the effects of clouds on solar power production could be analyzed more accurately. If high correlations were found between sites after the diurnal cycle had been removed, Long and Ackerman surmised that a large weather front with similar cloud type throughout had passed over the area. Thus, it is conceivable that an effective method for the

calculation of cloud size can be performed using correlation coefficient analysis. Overall, Long and Ackerman's relatively simple analysis showed many aspects of the intermittencies of solar power that need to be explored further.

Another two common forms of analysis of solar intermittency investigate ramp rates of power output (5). Ramp rates are defined as the differences in output over a given period divided by the duration of the period. These simple analyses can be used to construct a picture of how power output changes over different time periods. This will allow researchers to understand what types of supplementary power sources may be needed to compensate for intermittency, but also quantify the variation in output exhibited by the power source in question. Thus, the analytical techniques used by Wan to examine wind power can be easily applied to solar power research.

An analysis of the solar photovoltaic (PV) power output of four large-scale sites using power spectral density, as well as correlation and step size analyses, over both short and long time scales, was demonstrated in 2007 (3). Using this advanced analysis, a flatter power spectrum for solar power than for wind at the same location for fluctuations in the 10 minute to several hour range was calculated (3). This result implies that more supplementary power production would be needed to compensate for solar intermittencies in this frequency regime, relative to wind power, making solar power potentially more expensive. This research showed the importance of power spectrum analysis of solar power sites.

There is an entirely different approach to analyzing the intermittencies of solar power, as summarized by Woyte et al. in 2006, which involves the modeling of cloud movements and sizes (6). These methods range from simply assuming wind speeds and directions and calculating the average reduction of incident solar irradiation, to

more complex methods using fractals. Although understanding the movements and sizes of clouds does not completely describe the intermittency of solar power, the effects of cloud movement and size were found to be related to solar PV power output.

This paper will build upon the discussed research by analyzing a unique array of 8 sites that are spaced between 180 feet and 2.1 miles using 5 minute GHI data gathered over 5 months. One-to-one site comparisons and correlation analysis in both time and space will be used to determine the relations in GHI between each site. Ramp rate and step size analysis will be used to examine the variability of the GHI at each site. In addition, using an aggregate analysis, this project will characterize the GHI seen by the array of solar power sites as a whole, attempt to describe the array's power output and finally draw conclusions about the quality of net power output from a distributed array of solar power sites.

# 2. METHODS

## 2.1. The DEMROES wireless weather station network and its data

To accurately model a city's or a state's residential solar power systems, an array of sites that either are powered by or measure solar irradiation that are dispersed over an area of interest is desirable. Such an array exists on the campus of the University of California at San Diego and is run under the UCSD Decision Making Using Real-time Observations for Environmental Sustainability (DEMROES) project. A total of 8 of these stations are located on building tops around campus (see Figure 1), most free of obstruction from the Sun throughout the day. These stations are programmed to sample global horizontal irradiation (GHI) every second using a Licor 200X pyranometer and store the averaged data every 5 minutes.

Data gathered from this array of weather stations spanned the time frame of May 1, 2008 to November 2, 2008. Most of the 8 stations recorded long time periods of uninterrupted data during this time frame with notable exceptions detailed in Table 1.

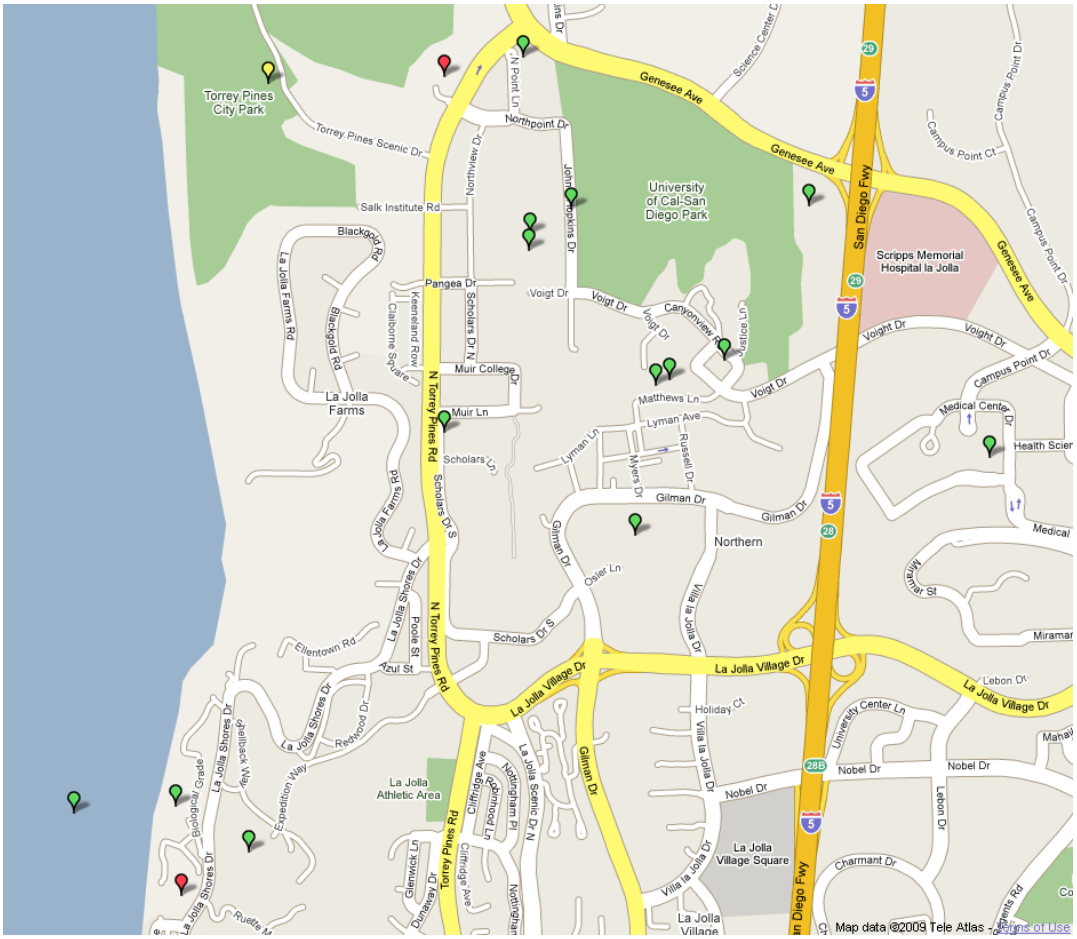


**Figure 1: Locations of DEMROES meteorological stations across the UCSD campus (green markers) on Google Maps. The dimensions of the map are 2 miles x 2 miles**

**Table 1: Description of GHI data availability at each site**

| Site | Time Period in 2008 | Description |
|---|---|---|
| **Hubbs Hall** | 5/01 to 7/20<br>7/21 to 7/28<br>7/29<br>7/30 to 10/20 | Complete<br>Missing morning and evening data<br>Missing morning data<br>Complete |
| **Tioga Hall** | 5/16 to 11/10 | Uninterrupted |
| **RIMAC** | 5/01 to 5/12<br>5/13 to 5/27<br>5/28 to 10/23 | Complete<br>Missing data<br>Complete |
| **Biomedical Science Bldg (BMSB)** | 5/01 to 11/02 | Complete |
| **CMRR** | 5/01 to 5/23<br>5/24 to 5/27<br>5/28 to 11/03 | Complete<br>No data<br>Complete |
| **Powell Structures Lab** | 6/18 to 10/10<br>10/11 to 11/13 | Complete<br>Missing some morning hours |
| **EBU2** | 5/01 to 11/02 | Complete |
| **Moores Cancer Center (MoCC)** | 5/01 to 10/20<br>10/21 to 11/02 | Complete<br>Missing morning and evening data due to shading |

## 2.2. Data Quality Control

Prior to the start of this paper's analysis, the data had been quality controlled by Professor Jan Kleissl. A cross-calibration was applied for the data at different sites to correct for accuracy in the factory-calibration of the sensors, dust loading, and inaccuracy in the leveling of the sensor. The cross calibration was determined from linear regression on 7 clear days throughout the data period. Since the sites were close together and nearly at the same elevation, it can be assumed that the SKC atmospheric transmittance is identical at all sites. Consequently the differences observed on clear days can be used to infer the measurement error at each site. For this calibration, the RIMAC sensor was randomly picked as the standard.

The data quality control does not take into account shading of the sensors. Shading occurs at large solar zenith angles when ground-based objects, such as topography, buildings, rooftop installations, or parts of the weather station itself are located between the Sun and the sensor. The locations that are expected to be free from shading errors are Tioga, RIMAC, EBU2, and BMSB. Other sites exhibit shading of varying severities and time periods. The details of shading at each site are detailed in Table 2.

**Table 2: Severity of shading at each site**

| Station | Shading Severity | Shading Time Periods | Reason |
|---|---|---|---|
| **Hubbs** | Minor | Morning | Topography to the east |
| **Tioga** | Zero | None | No shading |
| **RIMAC** | Zero | None | No shading |
| **BMSB** | Zero | None | No shading |
| **CMRR** | Moderate during 9/30 – 3/10 (est) | Morning | Powell east of CMRR is much taller |
| **Powell** | Moderate until 6/18 and 10/10 onward | Morning | SPN1 pyranometer shades Li200X pyranometer |
| **EBU2** | Zero | None | No shading |
| **MoCC** | Moderate 11/5 – 3/4, Severe near winter solstice | Morning and evening | Rooftop installation |

## 2.3. One-to-One Comparisons

In the analysis of the GHI data gathered at each location, a significant dimension is each site's distance from the coastline, as meteorological conditions are highly dependent on this value. Table 3 shows each site's distance to the coastline arranged in ascending distance from the ocean.

**Table 3: Distance to the coastline from each site**

| | **Hubbs** | **Tioga** | **RIMAC** | **BMSB** | **CMRR** | **Powell** | **EBU2** | **MoCC** |
|---|---|---|---|---|---|---|---|---|
| **Distance to Coastline (km)** | 0.09 | 0.89 | 1.31 | 1.69 | 1.78 | 1.84 | 2.07 | 3.17 |

The north-south distance between sites is not a significant consideration in this paper as the solar zenith angle, and thus the GHI, does not vary significantly across the distances between the sites. Additionally, the effects of proximity to the ocean greatly outweigh the effects of north-south distance between sites. However, neglecting north-south distances can introduce the occasion where two sites are a similar distance from the ocean, but a significant distance away from each other as the crow flies. This may occur between the Tioga and RIMAC locations or the RIMAC and Biomed locations.

To understand qualitatively the variations in GHI between the sites, scatter plots of the measured GHI at each site against the GHI measured at the Hubb site were created. Although these plots do not yield quantitative comparisons between the sites, they do allow an initial inspection as to how the GHI varies between the sites in general. For example, Figure 2 shows that while the GHI measured at the BMSB site tends to equal that measured at the Hubb site, when differing, the GHI at BMSB tends

to be larger than the Hubb site. This indicates the BMSB site experiences a clearer sky more frequently than the Hubb site.

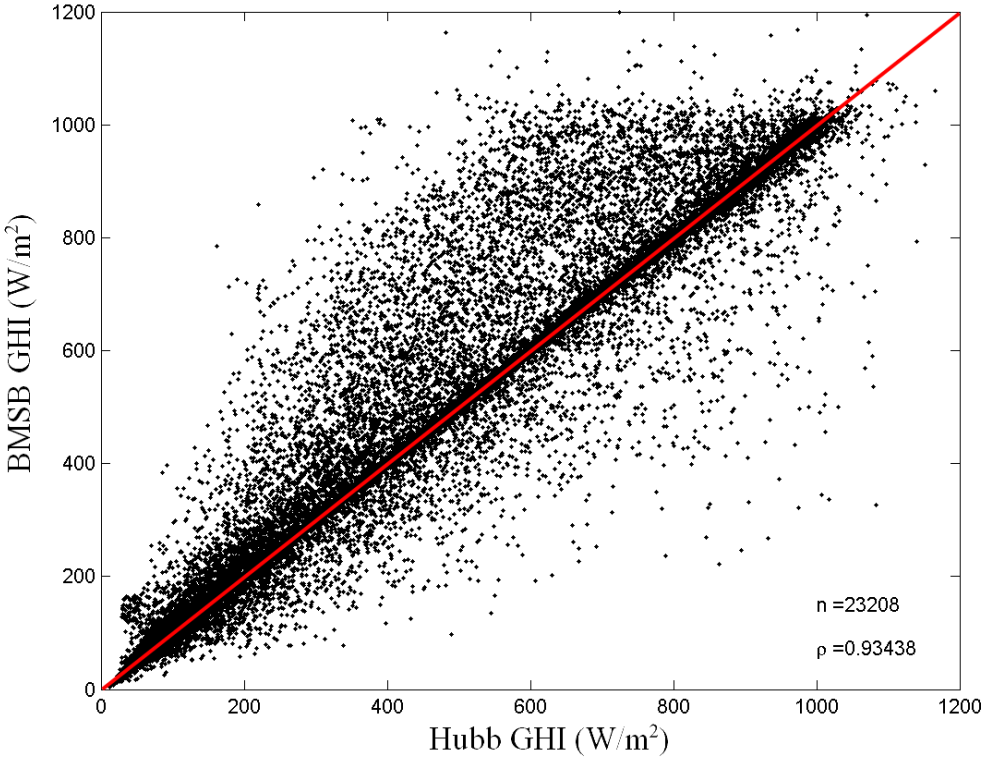


**Figure 2: GHI at BMSB versus GHI at Hubb with red 1:1 line. The text insert shows the number of 5 minute data points, n, and the correlation coefficient, ρ**

## 2.4. Clear-Sky GHI Profiles

Clear-sky GHI (SKCGHI) profiles can be used to normalize measured GHI at each site. SKCGHI is modeled by a power law equation of the form

$$\text{SKCGHI} = a{\mu_o}^b \quad (1)$$

where SKCGHI is the clear-sky global horizontal irradiation, $a$ and $b$ are regression coefficients and $\mu_o$ is the cosine of the solar zenith angle. The coefficient $a$ represents the clear-sky irradiation for a solar zenith angle of 0° and includes such effects as the average aerosol and column water vapor amounts, Earth-Sun distance, and radiometer calibration (7). The coefficient $b$ includes such effects as the radiometer cosine

response (7). This SKCGHI profile will be used to compare measured GHI data to an "ideal" maximum value representative of cloud-free conditions at a given time.

As Equation 1 shows, the SKCGHI profile for a given location on a given day can be obtained knowing the Sun's solar zenith angle and two regression coefficients. The solar zenith angle is defined as the angle between the local zenith (the point directly overhead) and the line of sight to the Sun. This is shown in Figure 3.

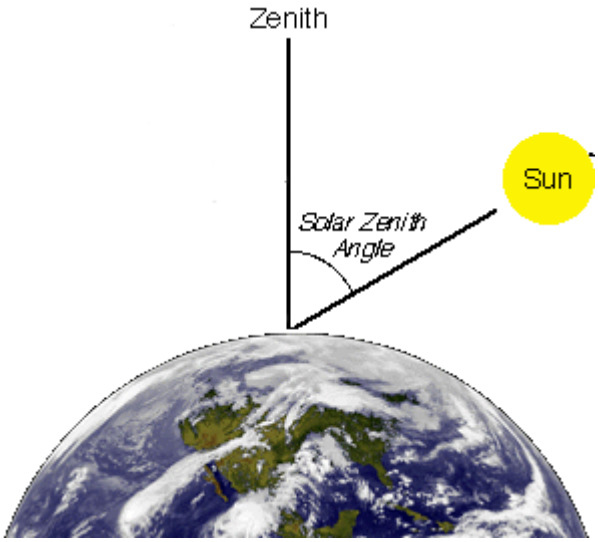


**Figure 3: Definition of solar zenith angle (8)**

Global and either the diffuse (DifSI) or direct (DirSI) solar irradiation measurements are required to obtain coefficients *a* and *b* (7). GHI and DifSI data from a Delta SPN1 pyranometer at the PoSL site was input to a program called "Sunny Days", created by Chris Gonzales and Steve Wilcox of the National Renewable Energy Laboratory (NREL) in Golden, CO., to calculate the regression coefficients of Equation 1.

The program was originally designed for SKC analysis at any site that collects GHI and DifSI or DirSI measurements (9). Inputs to the program included the measured GHI and DifSI from the Powell site, along with its latitude, longitude and elevation. The program identified SKC periods within the data using the power law

formula described in Equation 1 and additional aspects of Long and Ackerman's work (7; 9). Results are available for display in graphical form, as shown in Figure 4, and in the form of the desired coefficients of Equation 1. Using these coefficients, SKCGHI profiles for each day between May 1, 2008 and November 13, 2008 were created and later used as a reference for measured GHI data at each site. It is important to note that, due to the form of Equation 1, the error in the SKCGHI profiles is proportional to that of the pyranometer in measuring GHI and DifSI.

Figure 4 shows an example output from the Sunny Days program. Using the inputs of GHI and DifSI, the program calculated DirSI by the formula

$$\text{DirSI} = \text{GHI} - \text{DifSI} . \qquad (2)$$

The program then applied the power law (Equation 1) to the data to calculate the SKCGHI curve. The program also identified clear-sky portions of the input data.

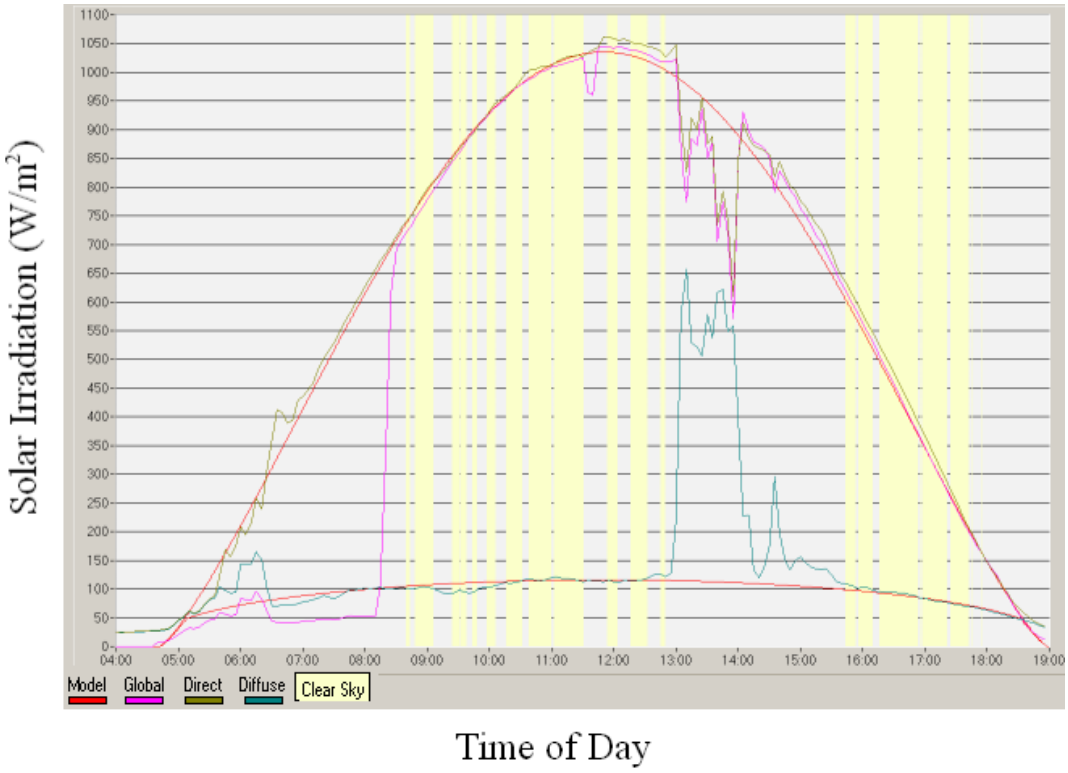


**Figure 4: NREL "Sunny Days" software output of SKCGHI for June 11, 2008. GHI is shown in pink, DifSI in teal, DirSI in green, and SKCGHI in red. SKC periods are highlighted yellow.**

Because solar zenith angle is a function of location, the coordinates of each site were used to calculate the solar zenith angles input to Equation 1, which resulted in unique clear-sky curves for each site. This increased the accuracy of the clear-sky curve modeling. However, it is important to note that the regression coefficients used were only calculated based on GHI and DifSI data collected at the PoSL site. This resulted in a slight inherent error; however, due to the close proximity of the sites, this error can be considered negligible. An improvement of these calculations could be accomplished by collecting DifSI and GHI data at every site. However, this would require significantly more equipment and is beyond the scope of this project.

## 2.5. Daily Stratification by Cloudiness

To provide additional insight into the character of the GHI experienced at each site, each day was classified as sunny, intermittently cloudy or cloudy using its clear-sky fraction. The calculation of a day's SKC fraction is begun by determining the SKC fractions for all 5 minute intervals during that day. This is accomplished by

$$f_t = \mathrm{GHI}_t / \mathrm{SKCGHI}_t \tag{3}$$

where $f_t$ is the fraction of Sun on a given 5 minute interval, $\mathrm{GHI}_t$ is the measured GHI at that 5 minute interval and $\mathrm{SKCGHI}_t$ is the modeled SKCGHI at that 5 minute interval. After all 5 minute SKC fractions were calculated for a given day, the SKC fraction of that day was calculated by averaging all of its 5 minute clear-sky fractions. The result is the average fraction of SKC experienced at that site on that given day, *f*.

A day was considered sunny for $f > 80\%$, intermittently cloudy for $80\% > f > 55\%$ and cloudy for $f < 55\%$[1]. Figures 5a-c show examples of each of these days.

a) b) c)

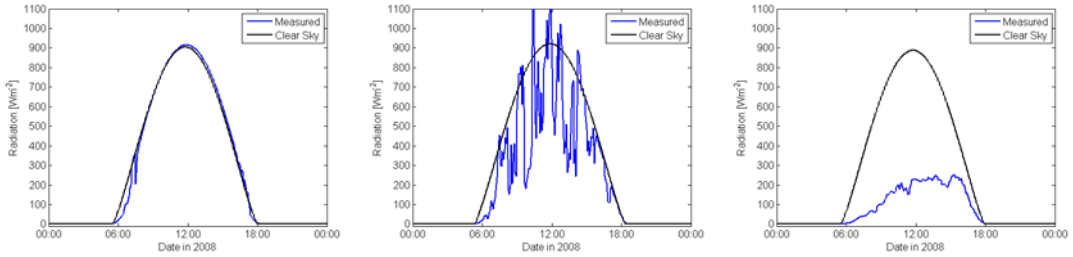


**Figures 5a-c: Example plots of GHI with overlaid SKCGHI profiles for days with different cloudiness: a) sunny; b) intermittently cloudy; and c) cloudy**

This stratification of days by cloudiness is an important and unfortunately somewhat subjective aspect of this project. The thresholds set for the fraction of sun used to stratify the analyzed days into sunny, intermittently cloudy or cloudy categories were selected based on common sense. Different thresholds were tested; however, the selected thresholds were chosen based on extensive visual examination of individual days' GHI, which focused on the character of GHI variations.

## 2.6. Correlation Coefficient Analysis

To compare the GHI measured at different sites, a correlation coefficient analysis was performed. This analysis described the relationship between each site's measured GHI and the GHI measured at the Hubb site. This site was chosen as the

[1] Another method of stratifying by cloudiness is to compute the total solar energy incident during a day on a unit area and compare that value to the SKC solar energy incident on the same area during the same day. This integration method requires similar thresholds to select the cloudiness for each day and thus yields similar results as the employed SKC-fraction method. However, days would be described by the delineation of energy instead of the fraction of sun, a potentially more useful measure.

benchmark site because it is nearest to the ocean and is therefore most affected by coastal weather phenomena.

A linear correlation coefficient is defined as a number that indicates the degree of dependence between two variables. The more dependent they are, the closer the value of the correlation to one (10). The correlation coefficient is calculated by

$$r = \frac{\sum xy}{\sqrt{\sum x^2 \sum y^2}} \quad (4)$$

where $r$ is the linear correlation coefficient, and $x$ and $y$ are the variables whose correlation is being calculated (11). For this project, $x$ and $y$ are the measured GHI of two different sites.

Correlation coefficients were calculated for days with each type of cloudiness (sunny, intermittently cloudy and cloudy) to yield more insight into the differences in GHI under difference types of cloudiness. Similarly, correlation coefficients were calculated by season, namely summer and fall.

## 2.7. Ramp Rate and Step Size Analysis

Ramp rate (RR) and step size (SS) analysis was used to analyze the variability of GHI at each site. SS is defined as the difference between two measured GHI data between a given time interval *dt*. RR is then simply the SS divided by the time interval *dt*.

When a probability density function (PDF) is applied to the calculated RR and SS, the resulting plot shows how the GHI varies most frequently. Since it is normalized, the PDF also allows the comparison of RR and SS between sites, regardless of data set size. Figure 6 shows an example plot of RR and SS. Both linear and semilogarithmic scales have been used: a linear scale emphasizes the

difference between days of different cloudiness, while a semilog scale displays the frequency of larger RR more clearly.

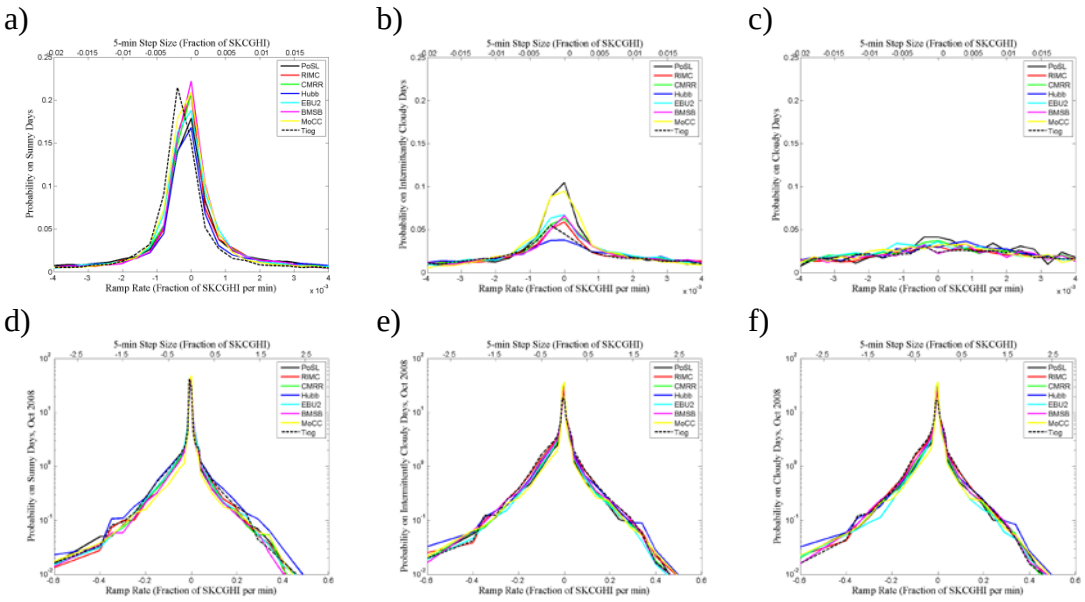


**Figure 6a-f: Example plots of RR and SS at all sites, plotted on linear and semilog scales, stratified by cloudiness: a,d) sunny; b,e) intermittently cloudy; c,f) cloudy**

As with the correlation analysis, comparing the RR PDFs of sites near the ocean against sites more distant from the ocean yields insight into how GHI fluctuations vary with proximity to the ocean. Additionally, RR and SS were calculated for each type of cloudiness and by season.

To understand the effect of the number of solar-producing sites on a distributed array's power production, aggregate RR and SS were also calculated. The one-station aggregate was computed by appending the normalized GHI at each site and calculating the RR PDF of the aggregate. The two-station aggregate was computed by first averaging the normalized GHI of all unique pairs of sites, appending the resulting data sets and calculating the RR PDF of the aggregate. The remaining aggregate RR PDFs, from the three-station through the eight-station, were calculated using a similar method. These aggregate RR are displayed on a semilog plot to emphasize how an increasing number of sites affects the array's net power

output. Additionally, to quantify the variability of the aggregate, the kurtosis (4th moment) and variance (2nd moment) of each aggregate's RR were also calculated. Example plots from this analysis are shown in Figures 7 and 8.

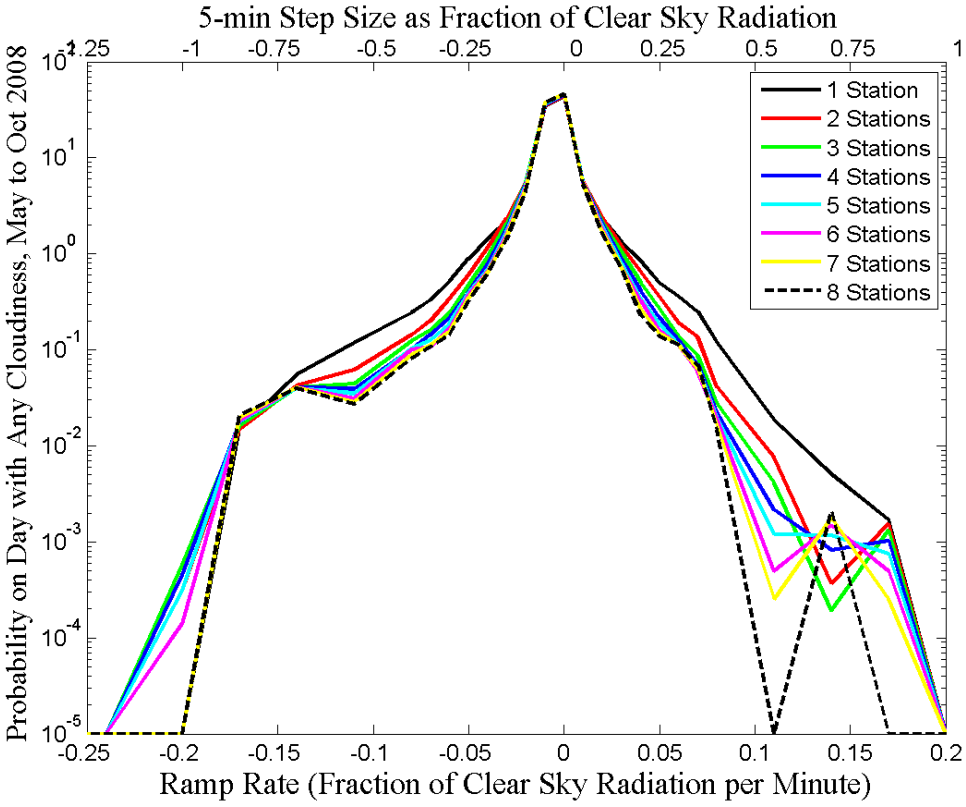


**Figure 7: Example plot of aggregate RR and SS for days with any cloudiness during May through October 2008, plotted on semilog scale**

a) b)

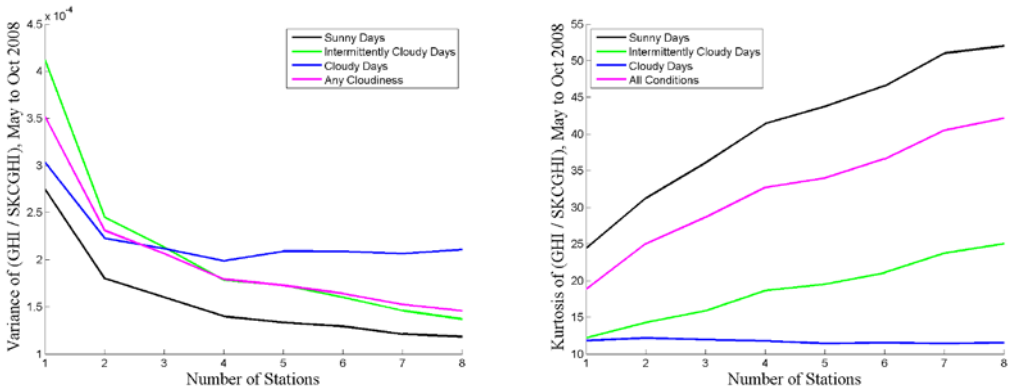


**Figure 8a,b: Example plots of aggregate a) variance; and b) kurtosis for days with any cloudiness during May through October 2008**

# 3. RESULTS

## 3.1. Background Research

As this project has built upon many years of research completed by Prof. Jan Kleissl of the University of California, San Diego, it is appropriate to detail his results thus far and appropriately set the stage for this paper's results. Figures 9 and 10a-j show the average GHI by month for the sites investigated in this paper. Note that Figures 10b-j are located in the Appendix.

Figure 9 shows that all sites exhibit the expected higher average daily GHI during the summer months and a lower GHI during the winter months. However, it is also shown that throughout the year, the Hubb site has almost consistently the lowest average daily GHI, while the MoCC site has almost consistently the highest. The remaining sites fall somewhere in between these two sites. Generally, this confirms what is already known about this geographic region: the coastal atmosphere has on average a lower transmissivity than more inland sites, which is caused by clouds and fog, due to the increased moisture content of the air near the ocean. This decreased atmospheric transmissivity causes the reduced GHI shown in the Hubb site GHI.

However, the data also show that the difference between the average daily GHI at the Hubb and MoCC is largest during the summer months of June, July and August. This is caused by the persistent coastal summer morning clouds, which persist longer at the coast than further inland.

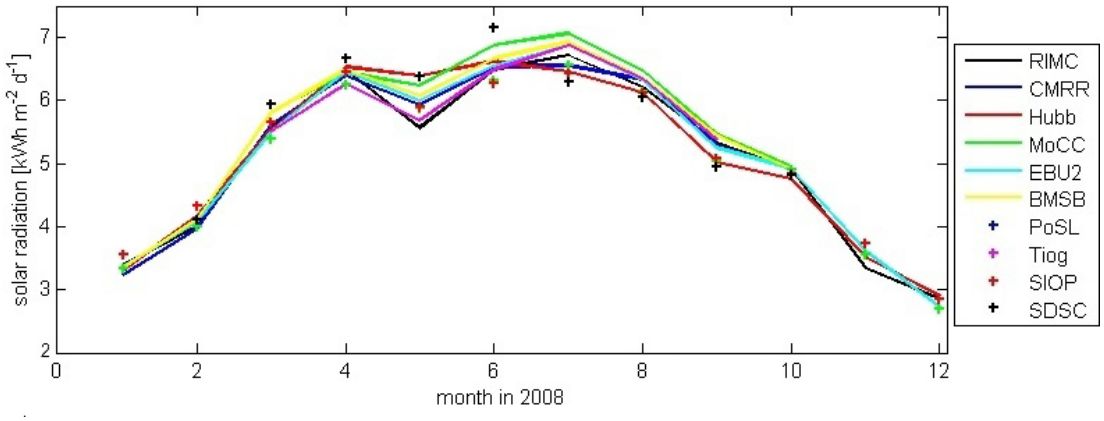


**Figure 9: Average daily GHI by month for 8 sites around UCSD during 2008**

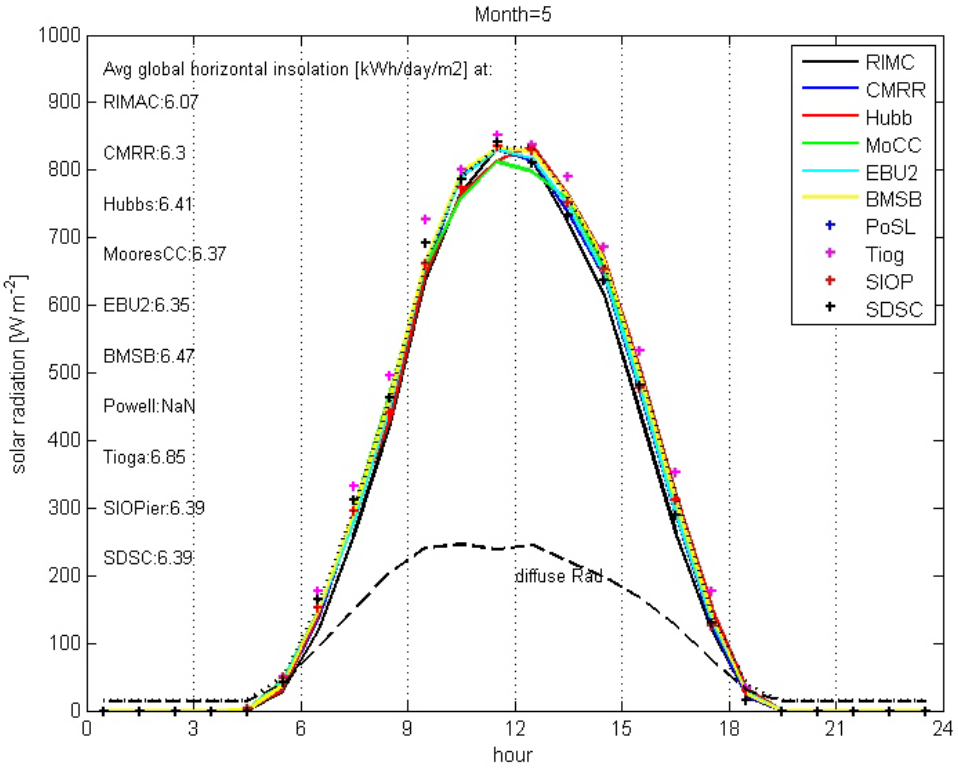


**Figure 10a: Average hourly solar irradiation flux by hour in May, 2008**

## 3.2. Stratify by Cloudiness

Table 4 shows information regarding the counts of days with different types of cloudiness, segregated by month, season and totaled. Average values and standard deviations are also included for comparison.

When considering the complete dataset from May to October, more sunny days are observed at more inland sites, particularly at EBU2 and Moore. However, on shorter time scales, the distribution of sunny and cloudy days is more random.

October is shown to be the least cloudy month, having only one cloudy day at one site, while July recorded the most cloudy days.

Additionally, more sunny days were recorded during fall than summer. The reverse is true for cloudy days, while intermittently cloudy days were nearly equal between the two time periods. This was probably caused by more persistent coastal fog conditions during summer, called “May gray” or “June gloom” by the locals.

**Table 4: Number of sunny, intermittently cloudy and cloudy days for each month, season and throughout May through October, as calculated by thresholds and SKC model described, with standard deviations, average values and totals. Sites with incomplete data records are marked in red italics.**

| | | Hubbs | Tioga | RIMAC | Biomed | CMRR | Powell | EBU2 | Moore | Average | Standard Deviation | Total |
|---|---|---|---|---|---|---|---|---|---|---|---|---|
| **May** | Sunny | 21 | 10 | *8* | 17 | 16 | *0* | 19 | 17 | 13.5 | 7.0 | 105 |
| | Intermittently Cloudy | 4 | 4 | *2* | 6 | 5 | *0* | 4 | 5 | 3.8 | 1.9 | 30 |
| | Cloudy | 6 | 3 | *7* | 8 | 7 | *0* | 8 | 9 | 6.0 | 3.0 | 48 |
| **June** | Sunny | 16 | 13 | 14 | 15 | 16 | *9* | 16 | 20 | 14.9 | 3.1 | 119 |
| | Intermittently Cloudy | 11 | 12 | 12 | 12 | 12 | *4* | 12 | 9 | 10.5 | 2.8 | 84 |
| | Cloudy | 3 | 5 | 4 | 3 | 2 | *0* | 2 | 1 | 2.5 | 1.6 | 20 |
| **July** | Sunny | 6 | 9 | 10 | 12 | 10 | 14 | 14 | 14 | 11.1 | 2.9 | 89 |
| | Intermittently Cloudy | 14 | 17 | 16 | 15 | 17 | 13 | 13 | 14 | 14.9 | 1.6 | 119 |
| | Cloudy | 3 | 5 | 5 | 4 | 4 | 4 | 4 | 3 | 4.0 | 0.8 | 32 |
| **August** | Sunny | 22 | 16 | 15 | 17 | 21 | 22 | 23 | 23 | 19.9 | 3.3 | 159 |
| | Intermittently Cloudy | 7 | 13 | 14 | 12 | 8 | 8 | 7 | 7 | 9.5 | 3.0 | 76 |
| | Cloudy | 2 | 2 | 2 | 2 | 2 | 1 | 1 | 1 | 1.6 | 0.5 | 13 |
| **September** | Sunny | 15 | 12 | 14 | 13 | 18 | 19 | 19 | 19 | 16.1 | 2.9 | 129 |
| | Intermittently Cloudy | 12 | 14 | 12 | 14 | 10 | 10 | 9 | 10 | 11.4 | 1.9 | 91 |
| | Cloudy | 3 | 4 | 4 | 3 | 2 | 1 | 2 | 1 | 2.5 | 1.2 | 20 |
| **October** | Sunny | 15 | 24 | 17 | 24 | 24 | 22 | 24 | 14 | 18.8 | 6.2 | 150 |
| | Intermittently Cloudy | 5 | 7 | 6 | 7 | 7 | 8 | 7 | 17 | 9.8 | 6.2 | 78 |
| | Cloudy | 0 | 0 | 0 | 0 | 0 | 1 | 0 | 0 | 0.1 | 0.4 | 1 |
| **Summer** | Sunny | 43 | 32 | 32 | 44 | 42 | 23 | 49 | 51 | 39.5 | 9.6 | 316 |
| | Intermittently Cloudy | 29 | 33 | 30 | 33 | 34 | 17 | 29 | 28 | 29.1 | 5.4 | 233 |
| | Cloudy | 12 | 13 | 16 | 15 | 13 | 4 | 14 | 13 | 12.5 | 3.7 | 100 |
| **Fall** | Sunny | 52 | 52 | 46 | 54 | 62 | 49 | 66 | 56 | 54.6 | 6.6 | 437 |
| | Intermittently Cloudy | 24 | 34 | 32 | 33 | 25 | 40 | 23 | 34 | 30.6 | 6.0 | 245 |
| | Cloudy | 5 | 6 | 6 | 5 | 4 | 3 | 3 | 2 | 4.3 | 1.5 | 34 |
| **May through October** | Sunny | 95 | 93 | 78 | 99 | 107 | 73 | 117 | 107 | 96.1 | 14.9 | 769 |
| | Intermittently Cloudy | 53 | 69 | 62 | 68 | 60 | 66 | 52 | 63 | 61.6 | 6.4 | 493 |
| | Cloudy | 7 | 19 | 22 | 20 | 17 | 10 | 17 | 16 | 16.0 | 5.1 | 128 |

### 3.3. Qualitative Site-by-Site Comparisons

Figures 11a-g show plots of each site's measured GHI versus the measured GHI at Hubbs. The purpose of these graphs is to check the quality of the GHI data gathered at each site and describe the relationships between the sites' measured GHI. This relationship is well described by the density of points along the 1:1 line: a denser cloud along the 1:1 line signifies a higher correlation between the two sites. Most observations at different sites are similar the majority of the time, lying along the 1:1 line and indicating high correlation. This is expected because the close proximity of the sites should result in little difference in average atmospheric transmissivity between the sites. It can also be seen that the data points not on the one-to-one line in the plots tend towards the left side of the plots, indicating higher GHI at another site in comparison to the Hubbs site.

The plots show that Tioga shows the highest correlation with Hubbs, which corresponds to it being the closest site to the ocean and to Hubbs. Conversely, MoCC shows the lowest correlation with the most points scattered towards the left of the 1:1 line. This indicates that the measured GHI at MoCC was frequently larger than at Hubbs, or, alternatively, that Hubbs was frequently more cloud-covered than MoCC, exemplifying MoCC's most inland location and its subsequently sunnier weather. Other sites show patterns similar to MoCC, but with a less dense cloud of points left of the 1:1 line, indicating a higher correlation with Hubbs and also more frequent cloud cover than at MoCC.

Figures 12a-g show the measured GHI less the modeled SKCGHI at each site versus the same measure at Hubbs. These plots display the already established 1:1 correlations between Hubbs and the other sites. However, an additional cloud of points can be seen along a horizontal line, for which Hubbs experienced a less-than-

SKCGHI while the other sites experienced a near-SKCGHI. This is most prominently exhibited in Figure 12e (MoCC). The density of this point cloud reduces significantly as the sites near the ocean, and nearly disappears in Figure 12c (Tioga). In Figure 12h, which compares the measured GHI less the modeled SKC at the BMSB site to that of the EBU2 site, this phenomenon vanishes and BMSB data is nearly always similar to the EBU2 data. This is caused by the sites' proximity to each other, as well as their similar proximity to the ocean (1.69 and 2.07 miles, respectively), which implies similar meteorological conditions.

Note that some data points in Figures 12a-g are positive, indicating a measured GHI which is larger than the SKCGHI. This is caused by some inaccuracies in calculating the SKC profile and by reflection of solar radiation off of nearby clouds, which can temporarily enhance GHI beyond the SKC value.

Figures 13a-g show plots of the normalized GHI at each site versus the normalized GHI at the Hubbs site. These plots are similar to Figures 11a-h and 12a-h, exhibiting both the 1:1 correlation and the horizontal axis point cloud discussed. However, the differences between the Hubbs site and the other sites are more pronounced, as the 1:1 correlations and horizontal axis density is more visible. For example, in the Tioga and RIMC plots (Figures 13c and 13g, respectively), the 1:1 correlations are obvious, while the horizontal axis densities are very low, as compared with Figures 12c,g. Conversely, in the MoCC and EBU2 plots (Figures 13d,e), the horizontal axis density is prevalent, while the 1:1 correlations are subdued, as compared with Figures 12d,e.

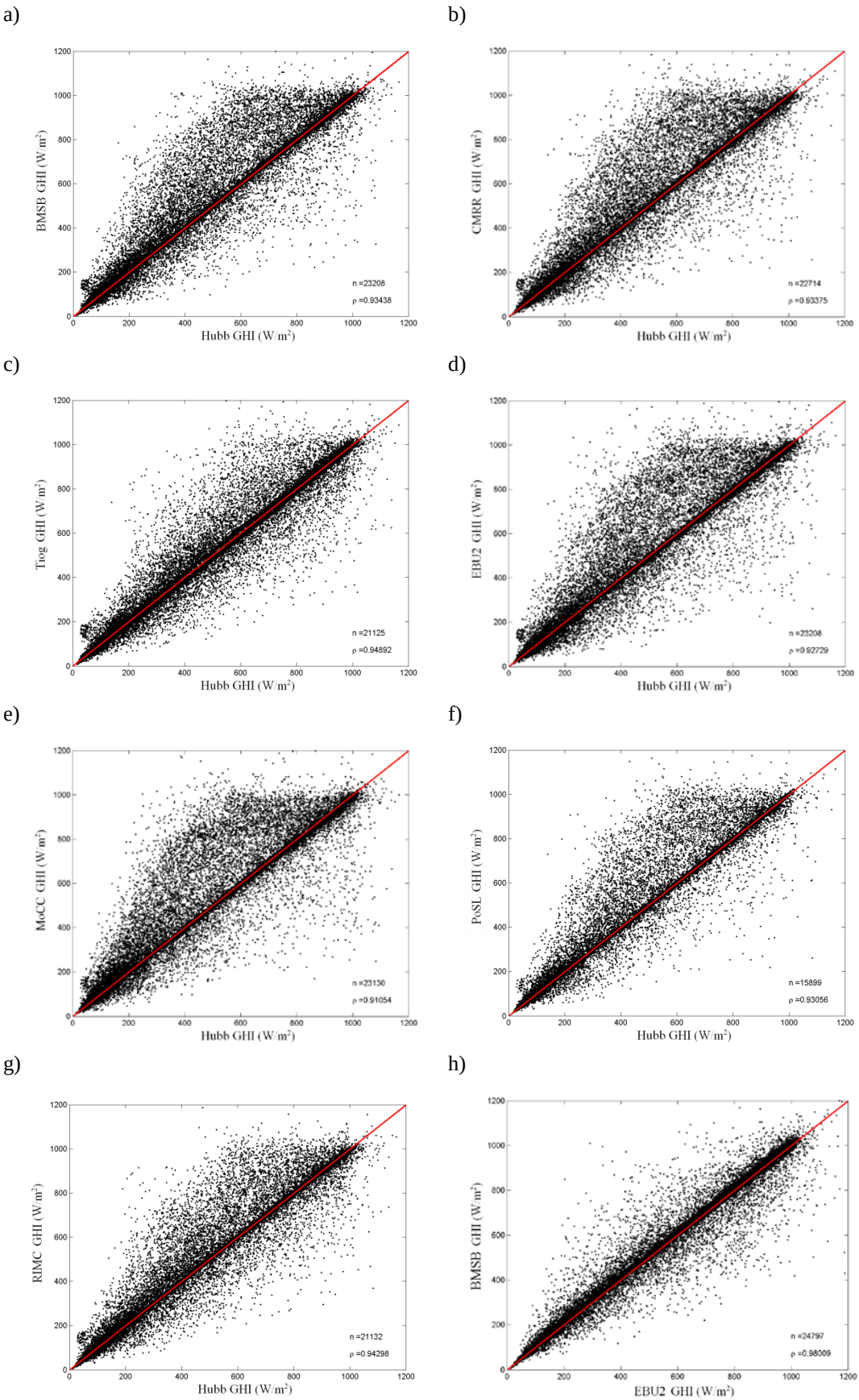


**Figures 11a-h: Scatter plots of all 5 minute averages of measured GHI: a-g) at each site versus Hubbs; h) at BMSB versus EBU2**

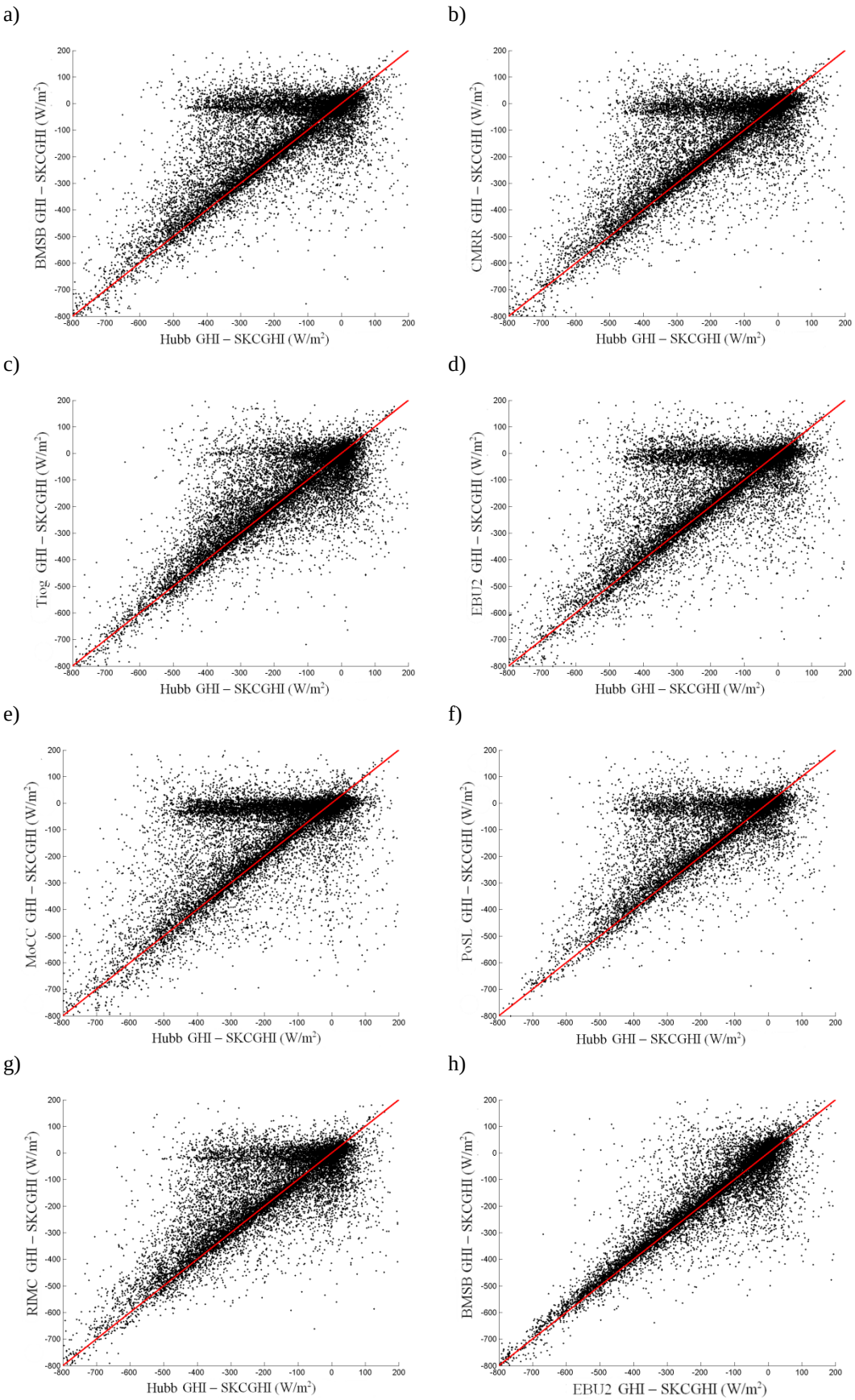


**Figures 12a-h: Scatter plots of all 5 minute averages of measured GHI with SKCGHI removed: a-g) at each site versus Hubbs; h) at BMSB versus EBU2**

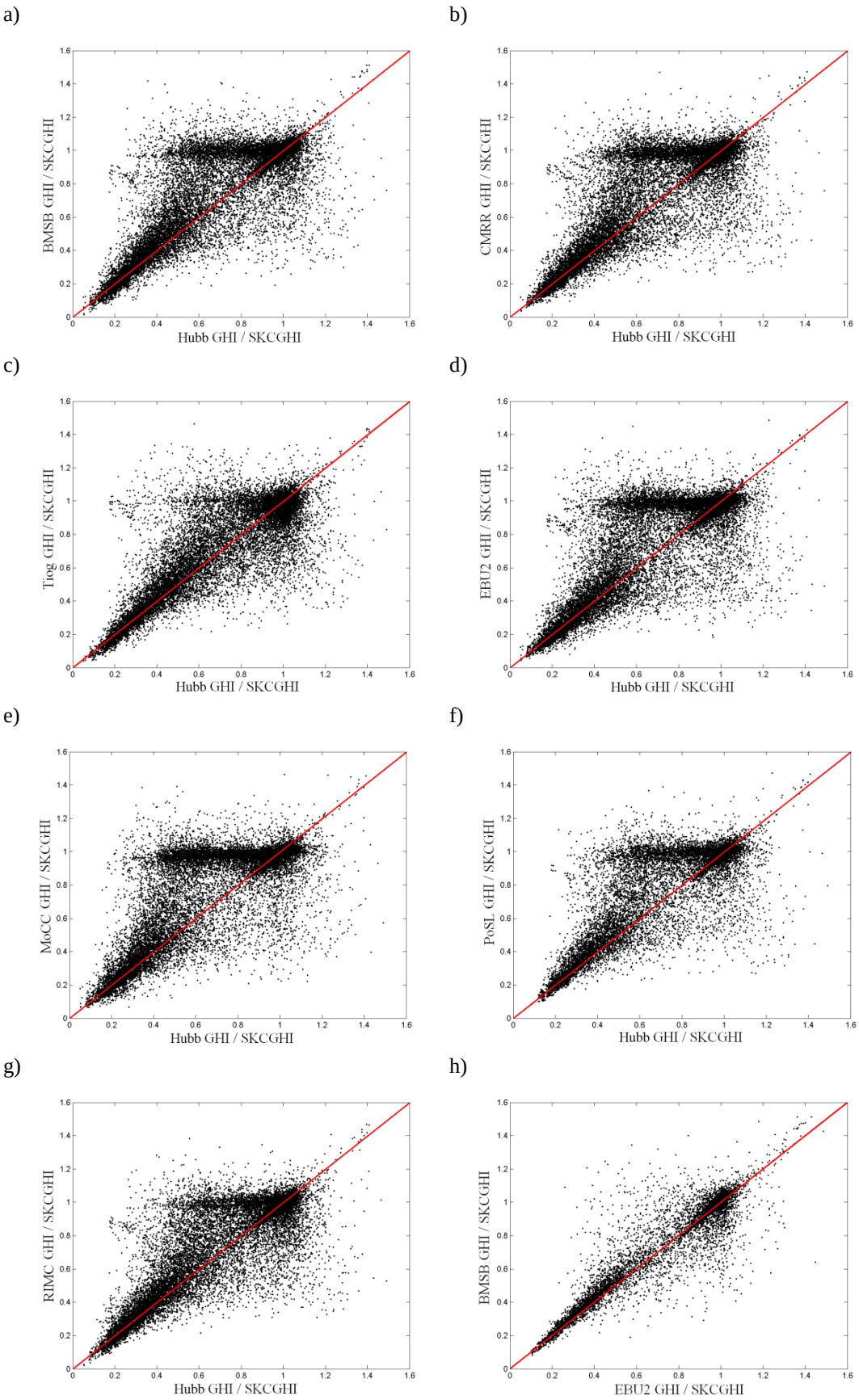


**Figures 13a-h: Scatter plots of all 5 minute averages of GHI / SKCGHI: a-g) at each site versus Hubbs; h) at BMSB versus EBU2**

## 3.4. Correlation Analysis

Figures 14a and 14b show how correlation coefficients change when SKCGHI is subtracted from measured GHI. As expected, the correlation coefficient between the sites' GHI is high across the time frame May through October 2008, never below 0.8. However, for GHI–SKCGHI, the correlation coefficients are significantly smaller since the differences between the sites are not masked by the similar diurnal cycle of the solar zenith angle. Effectively, removing SKCGHI from the calculations accentuates the effects of atmospheric transmissivity differences between sites.

Because the GHI at a given site depends on the local microclimate, which includes minute-to-minute variations in cloud cover, and other factors that influence atmospheric transmissivity (water vapor, aerosols, etc.), the correlation coefficients calculated between sites as distance between the sites is increased is expected to decrease (Figures 14a and 14b). When the diurnal cycle is removed, the decrease of correlation with distance becomes larger (Figure 14b), as expected.

It is important to note that on sunny days, correlation coefficients are expected to be high with a weak dependence on distance (Figure 14a). Additionally, intermittently cloudy days can be characterized by different methods depending upon what is being analyzed and can even be difficult to categorize, as discussed previously. Thus, the results of days with cloudy weather will be focused on in this section.

Correlation coefficients are shown to be slightly lower during the summer months as compared to the fall months for all types of cloudiness (Figures 15a-b). This implies that atmospheric transmissivity is more dependent on proximity to the ocean during the summer months than in fall months, which could be caused by

increased vapor content near the oceans due to higher temperatures during summer months.

On cloudy days, correlation coefficients decrease with distance from the ocean in similar magnitude throughout the summer months (Figures 16a-f). The correlation coefficients between the more inland sites and the more coastal sites are not significantly different from month to month.

It is shown that cloudy days have higher correlation coefficients than sunny and intermittently cloudy days (Figures 14b, 15a-b and 16a-f). This implies that the cloud cover on cloudy days is similar at all stations. Conversely, on sunny and intermittently cloudy days, cloud cover may be more random and not correlated across the sites, which would produce the lower correlation coefficients shown.

For this analysis, the weather at the Hubbs site was used to classify the results as occurring on either a sunny, intermittently cloudy or cloudy day. This was done to address the fact that, for example, a sunny day at one station was not necessarily a sunny day at another. Because the Hubbs site is located on the coast and used as a benchmark, this protocol was adopted.

a) b)

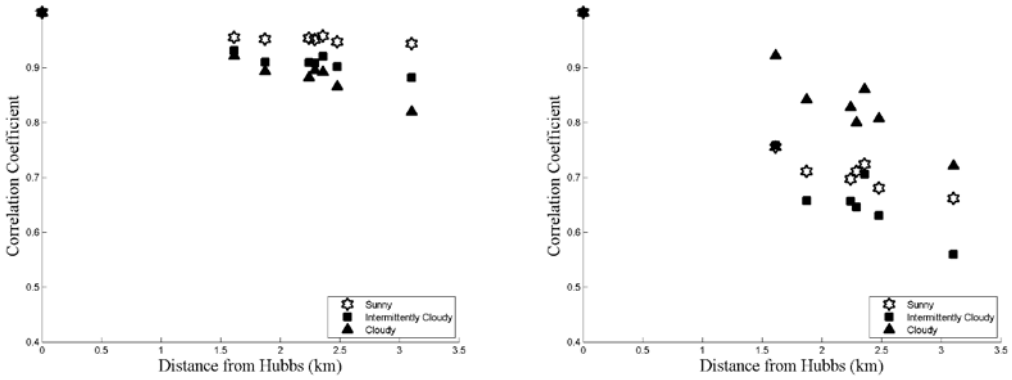


**Figure 14a-b: Correlation coefficients versus distance from Hubbs, May through October 2008: a) SKCGHI included; b) SKCGHI removed**

a) b)

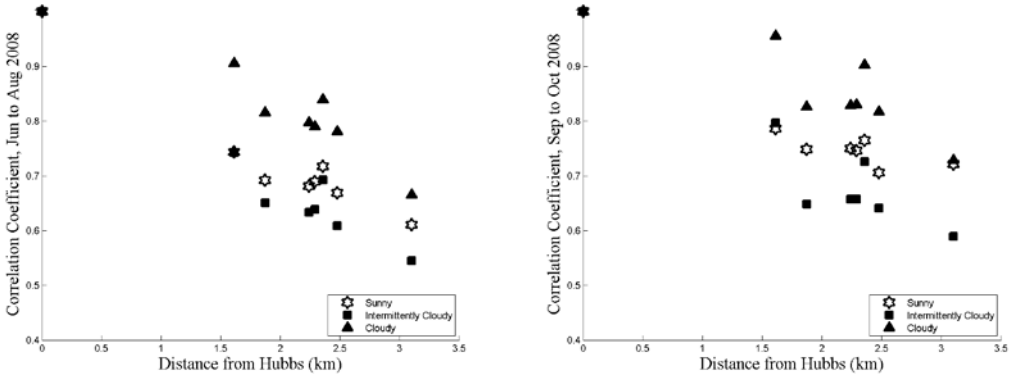


**Figures 15a-b: Correlation coefficients versus distance from Hubbs by season with SKCGHI removed**

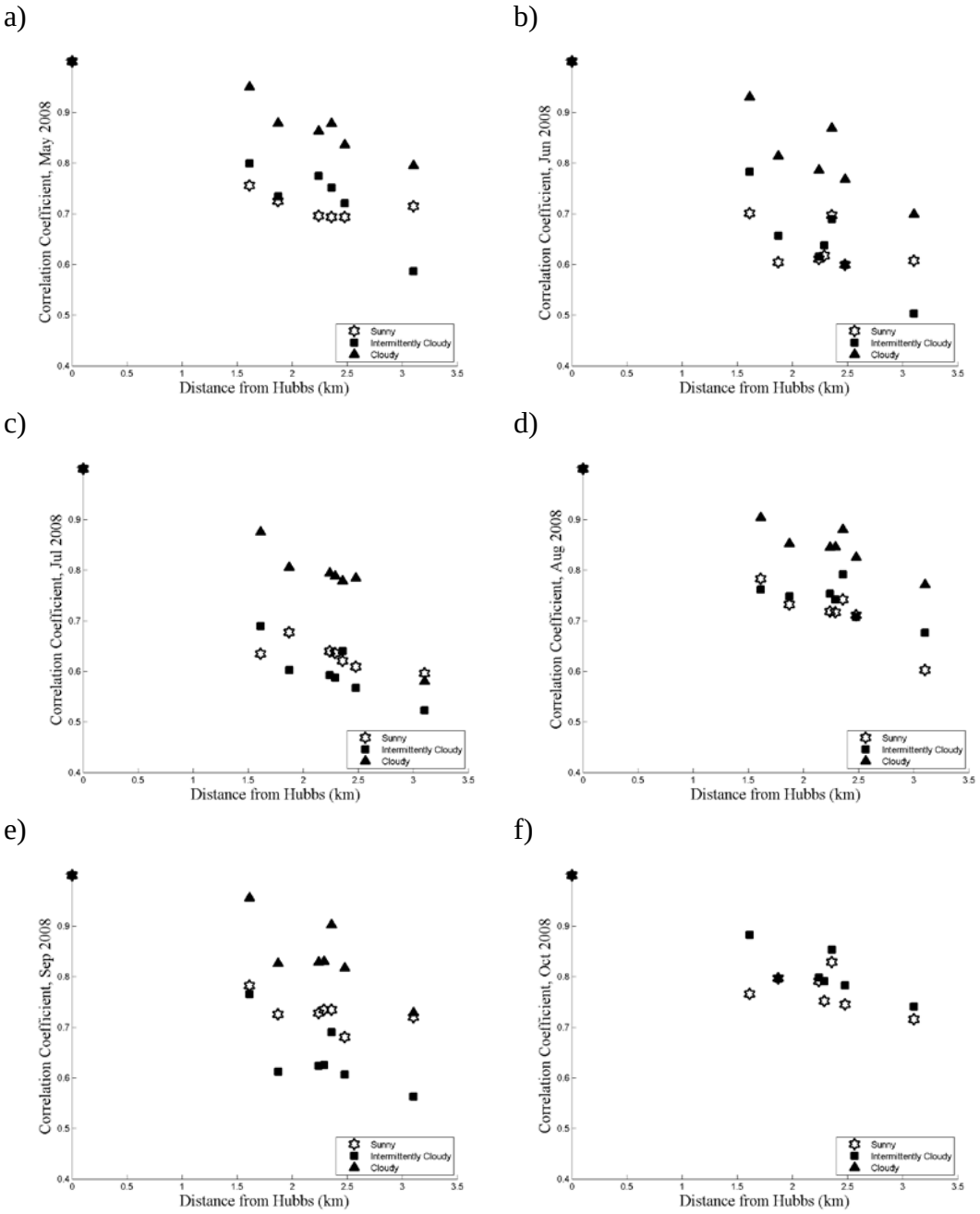


**Figures 16a-f: Correlation coefficients versus distance from Hubbs by month with SKCGHI removed. Note that too few cloudy days were recorded during October to calculate a correlation coefficient.**

## 3.5. Ramp Rate and Step Size Analysis – Individual Sites

Note that all step size (SS) and ramp rate (RR) plots are normalized to SKCGHI. Thus, RR can be thought of as a percentage of the SKCGHI at a given time. Figures 17a-h show the PDFs of SS and RR for each site, stratified by cloudiness from May through October 2008, plotted on both linear and semilog scales. On sunny days, it is shown that RR are more likely close to zero than on cloudier days (Figures 17a,c,e,g). This is because on clear days, the slow change in solar zenith angle dictates the RR at a given site instead of the more rapid fluctuations of GHI caused by passing clouds.

The SS and RR were also stratified by location (Figures 17a-h). For example, in Figure 17a, the probability of a RR close to zero is significantly higher at the most inland MoCC site as compared to the most coastal Hubbs site.

As shown in the semilog RR PDF plots (Figures 17b,d,f,h), the occurrence of large RR is shown to be frequently higher for more coastal sites, most prevalently on sunny days, but also on cloudier days. There also appears to be more uniformity in both small and large GHI RR experienced at all sites on cloudier days.

Table 5 shows the variance and kurtosis of RR calculated for each site. The variance is a standard measure of the variability of RR (and thus also of the measured GHI), while the kurtosis describes what type of deviations contribute to the variance: a larger kurtosis indicates that more of the variance is due to infrequent extreme deviations, as opposed to frequent modest deviations.

When considering days with any cloudiness, the RR variances are similar across all sites, with the exception of the Hubbs site, which has a significantly larger variance. This trend implies that cloud cover is more variable near the ocean, but becomes relatively constant in variability less than 1 km from the ocean.

The kurtosis of RR is shown to generally increase as distance from the ocean is increased. This implies that the character of the variability of inland sites is marked by more infrequent extreme deviations. It is reasonable, therefore, to surmise that inland sites may experience a higher occurrence of thick, scattered clouds passing overhead, as compared to a more constant and/or less dense cloud cover near the ocean.

These trends are similar for sunny days, which follow logically from the fact that a large percentage of the days in the data were sunny (see Table 4). However, the increasing trend of the kurtosis is more apparent on sunny days.

Intermittently cloudy days show a lessening of the increasing trend of the kurtosis as well as a less steep drop in the variance between the Hubbs site and the more inland sites. These trends, however, are shown to be stronger on cloudier days.

In stark contrast to sunny days, cloudy days show a relatively uniform variance across all sites, while their kurtosis is actually shown to decrease as distance inland is increased. This change in the behavior of the kurtosis, as compared to sunnier days, implies that the more coastal sites experience more frequent, larger jumps in RR than more inland sites on cloudier days.

The RR PDFs for the months of May through July (Figures 18a-d) and August through October (Figures 19a-d) are very similar to the overall results.

When the RR PDFs are shown separately for each month (Figures 20a-f), the months of May and June show more RR near to zero than the month of July, while October has significantly more RR near to zero than any other month examined. A large probability of RR near zero indicates less cloud cover and/or more persistent overcast clouds. A small probability of RR near zero indicates a month with more frequent and/or larger ramp rates. Consequently, it can be surmised that the month of

July experienced more patchy clouds than the months of May, June and October, while October had the clearest skies of them all. This determination is supported by the fact that October had nearly the most sunny days of any month (Table 4), which was probably caused by frequent Santa Ana conditions.

Additionally, RR at Hubbs typically has the smallest probabilities near zero. This implies that Hubbs experiences more frequent and/or larger RR due to its proximity to the ocean creating more varied cloud cover than any other site.

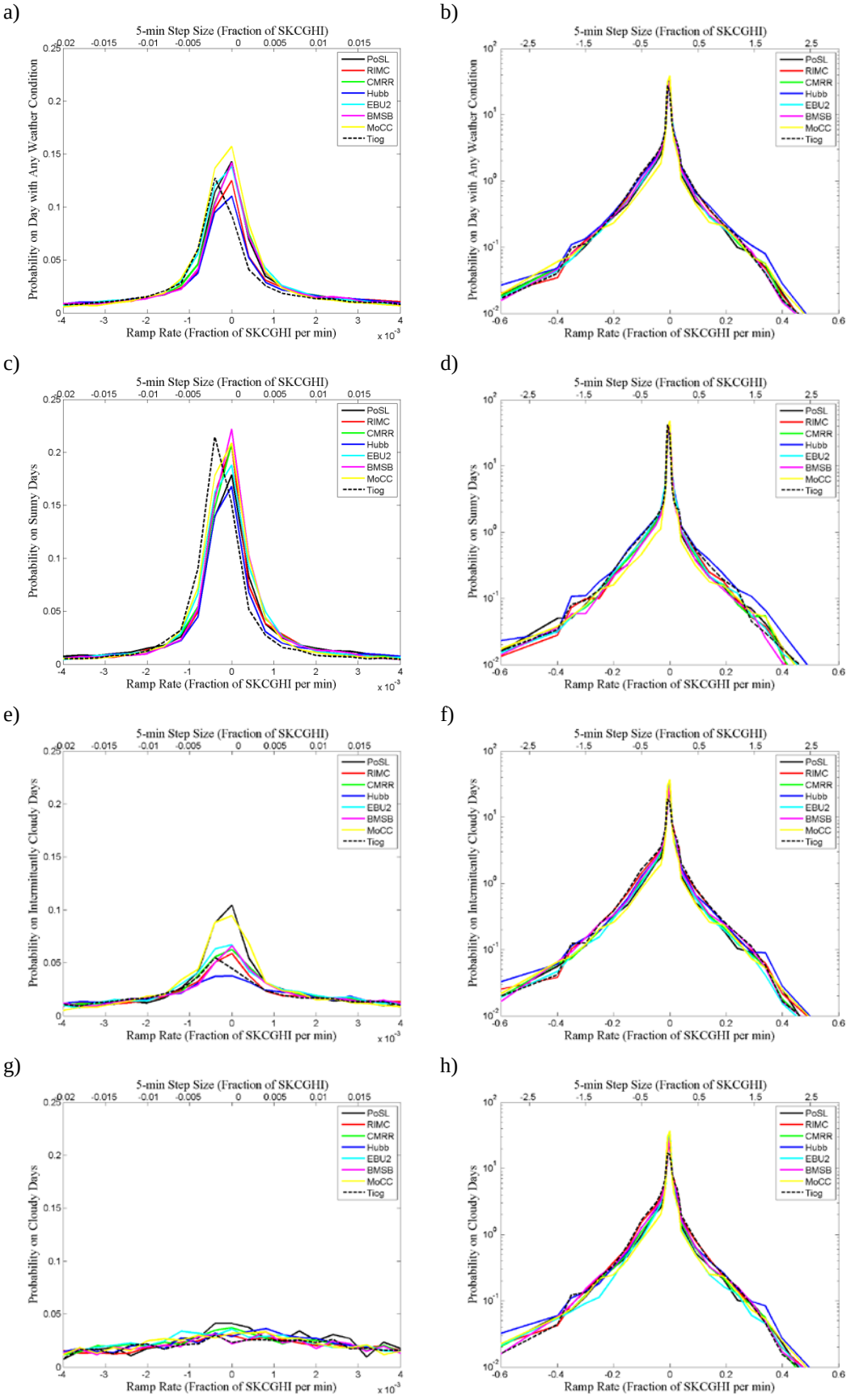


**Figure 17a-h: GHI RR and SS PDFs from May through October 2008 for all sites on days stratified as: a,b) any cloudiness; c,d) sunny; e,f) intermittently cloudy; and g,h) cloudy**

**Table 5: Statistical characteristics of GHI RR for each site, stratified by cloudiness for May through October 2008**

| | Ramp Rate Statistic | Hubbs | Tioga | RIMAC | Biomed | CMRR | Powell | EBU2 | Moore |
|---|---|---|---|---|---|---|---|---|---|
| **Any Cloudiness** | Variance ($min^{-2}*10^{-3}$) | 0.46 | 0.36 | 0.35 | 0.34 | 0.32 | 0.31 | 0.33 | 0.36 |
| | Kurtosis ($min^{-4}$) | 17.6 | 17.3 | 18.4 | 19.5 | 18.7 | 20.2 | 19.5 | 21.2 |
| **Sunny** | Variance ($min^{-2}*10^{-3}$) | 0.47 | 0.28 | 0.26 | 0.24 | 0.24 | 0.28 | 0.27 | 0.29 |
| | Kurtosis ($min^{-4}$) | 21.2 | 21.8 | 27.2 | 31.3 | 27.4 | 26.0 | 25.6 | 30.2 |
| **Intermittently Cloudy** | Variance ($min^{-2}*10^{-3}$) | 0.50 | 0.47 | 0.45 | 0.49 | 0.44 | 0.35 | 0.44 | 0.48 |
| | Kurtosis ($min^{-4}$) | 10.9 | 12.9 | 11.6 | 12.9 | 13.1 | 14.1 | 13.4 | 14.5 |
| **Cloudy** | Variance ($min^{-2}*10^{-3}$) | 0.34 | 0.29 | 0.27 | 0.32 | 0.34 | 0.38 | 0.34 | 0.42 |
| | Kurtosis ($min^{-4}$) | 28.0 | 17.8 | 13.3 | 13.3 | 14.0 | 12.1 | 13.0 | 13.1 |

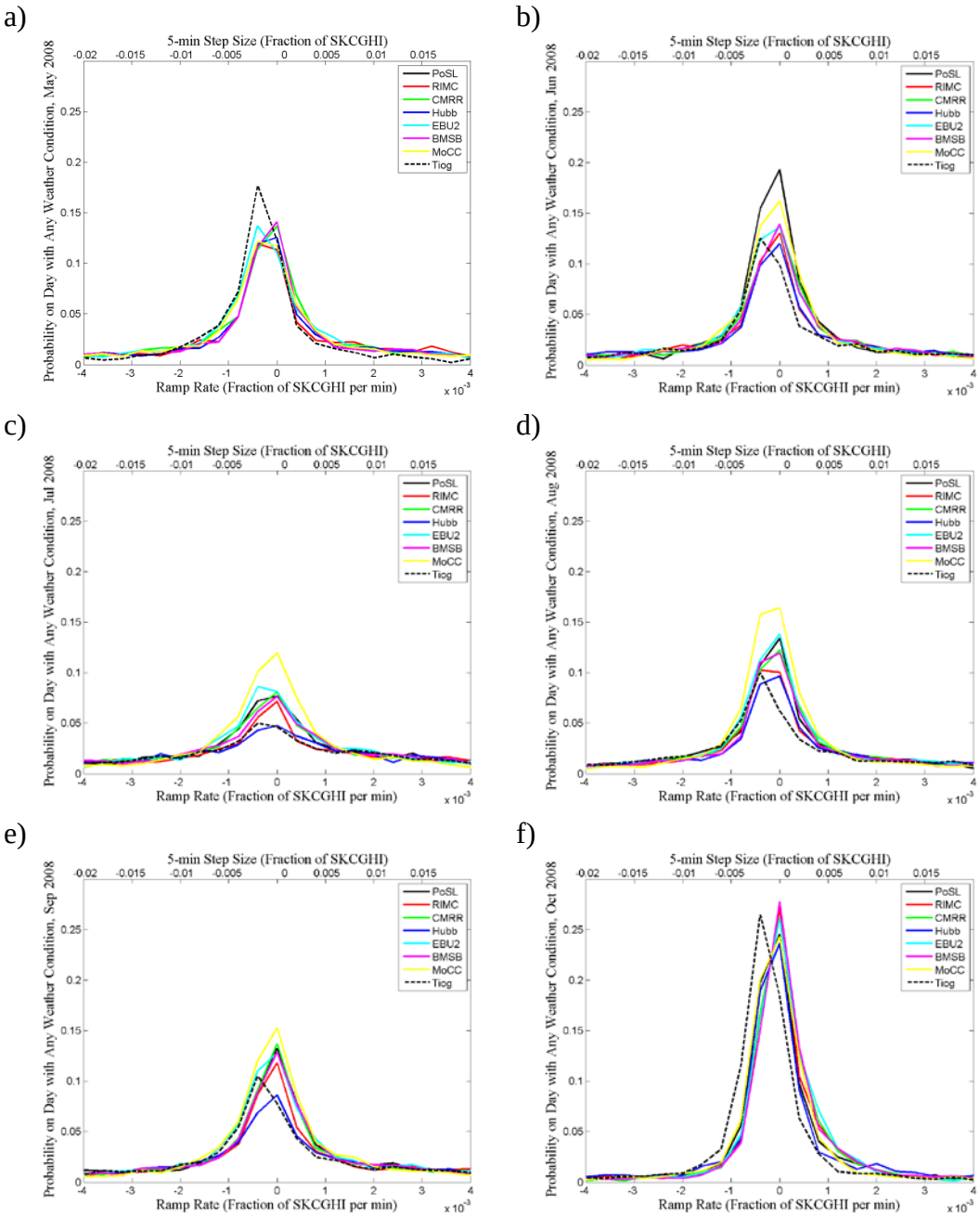


**Figure 20a-f: GHI RR and SS PDFs for all sites by month on days with any cloudiness**

## 3.6. Aggregate Ramp Rate and Step Size Analysis

Understanding the characteristics of aggregate RR is integral to answering this project's most important question: what qualities can be expected of the power output from a distributed array of solar sites. The net power produced by the array will be most sensitive to the average feed-in of solar power from all sites combined. It is obvious that this average feed-in will increase with the number of sites in the array; however, the characteristics of RR in relation to the number of sites in the array are not as clear.

In Figures 21a-d, it is shown that from May to October 2008, the RR and SS of the aggregate GHI reduces significantly as more sites are added to the aggregate. This implies that the frequency of large RR decreases as the number of sites present in a distributed array increases. Also, cloudier days exhibit a larger decrease in large RR frequencies than sunnier days as the number of sites in the aggregate is increased.

Variance of GHI RR is shown to decrease rapidly as sites are added to the aggregate and then more slowly after the aggregate exceeds four sites (Figure 22). Because this variance describes the dispersion of RR from SKC, the variance can be thought of as the deviation of the measured RR from the SKC RR profile: a higher variance indicates a more unpredictable and fluctuating profile than one with a low variance. Thus, an increase in the number of sites is shown to reduce the fluctuations in GHI of the distributed array as a whole.

Moreover, sunny days are shown to have the lowest variance, while cloudy days are shown to have the highest. This agrees with the physical situation and supports the results' validity. However, it is interesting to note that when the aggregate consists of only single stations, cloudy days have a variance near to that of

sunny days. This peculiarity exemplifies the necessity of understanding the relationship between the number of sites in an array and the array's net GHI RR.

Kurtosis of GHI RR on sunny days is shown to increase significantly with an increase in the number of sites in the aggregate, while cloudy days exhibit no change in kurtosis as the number of sites increases (Figure 23). This important result implies that the variance of GHI on sunny days is mostly caused by infrequent, yet large disturbances in GHI. This is indicative of a dense cloud or small, sparse patch of clouds passing over the site briefly. Additionally, the variance of GHI on cloudy days can be inferred to be caused by consistent deviations from SKCGHI, which is indicative of persistent cloud cover of constant opacity, such as a fog or a low stratus cloud layer.

Table 6 shows the numerical values of those plotted in Figures 22 and 23.

a)

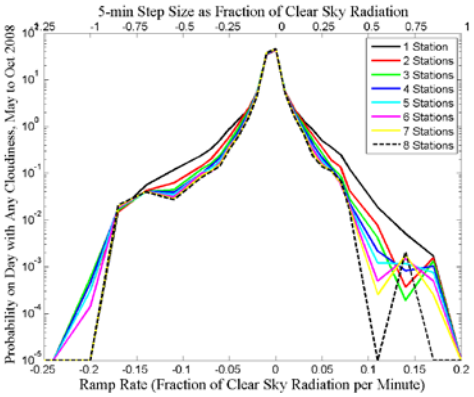


b)

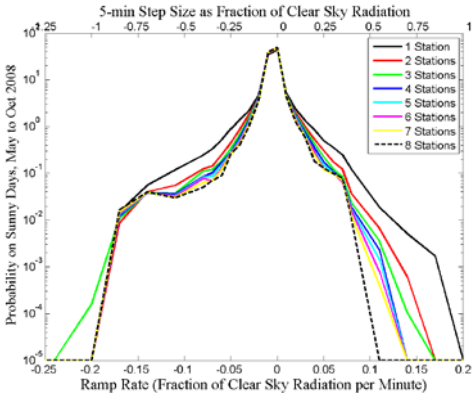


c)

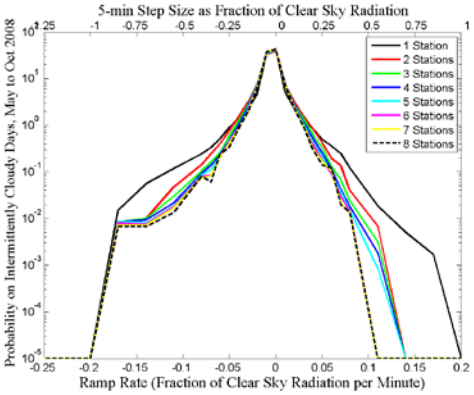


d)

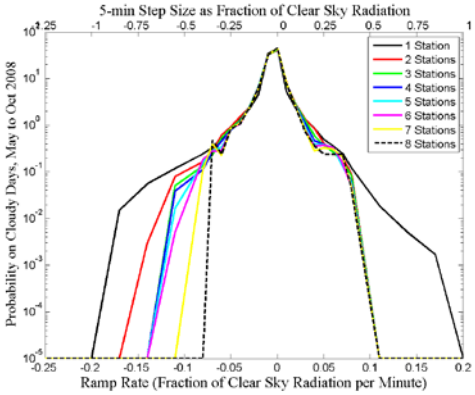


**Figure 21a-d: Aggregate RR and SS plots from May through October 2008 for days stratified as a) any cloudiness; b) sunny; c) intermittently cloudy; and d) cloudy**

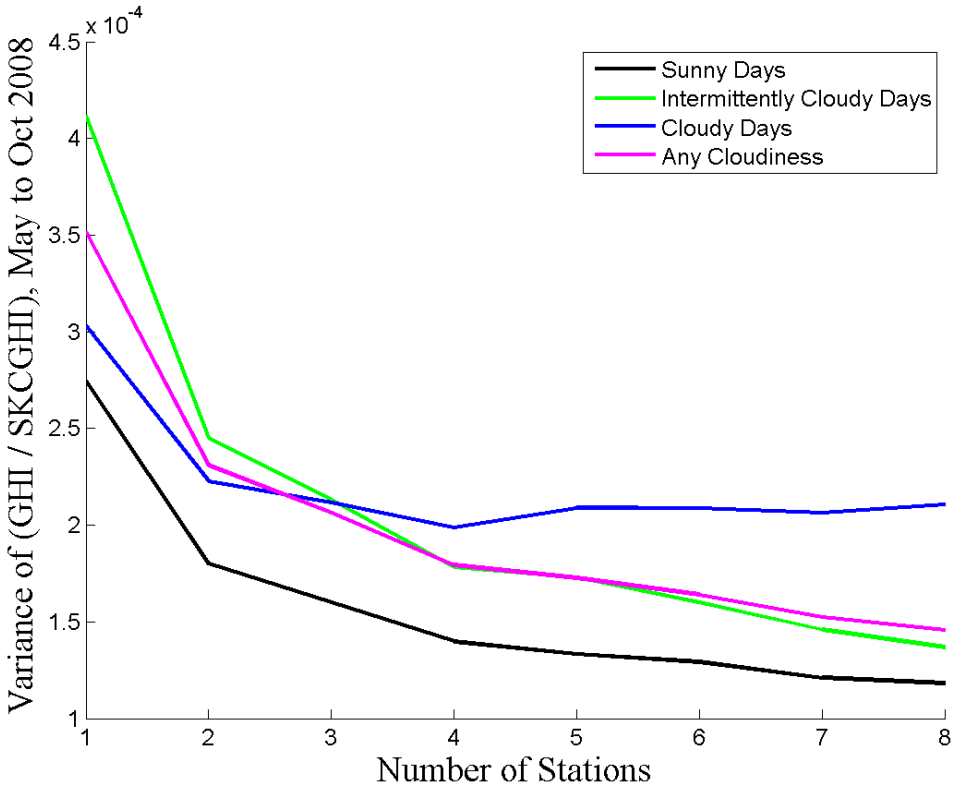


**Figure 22: Variance of aggregate GHI RR at all sites from May to October 2008**

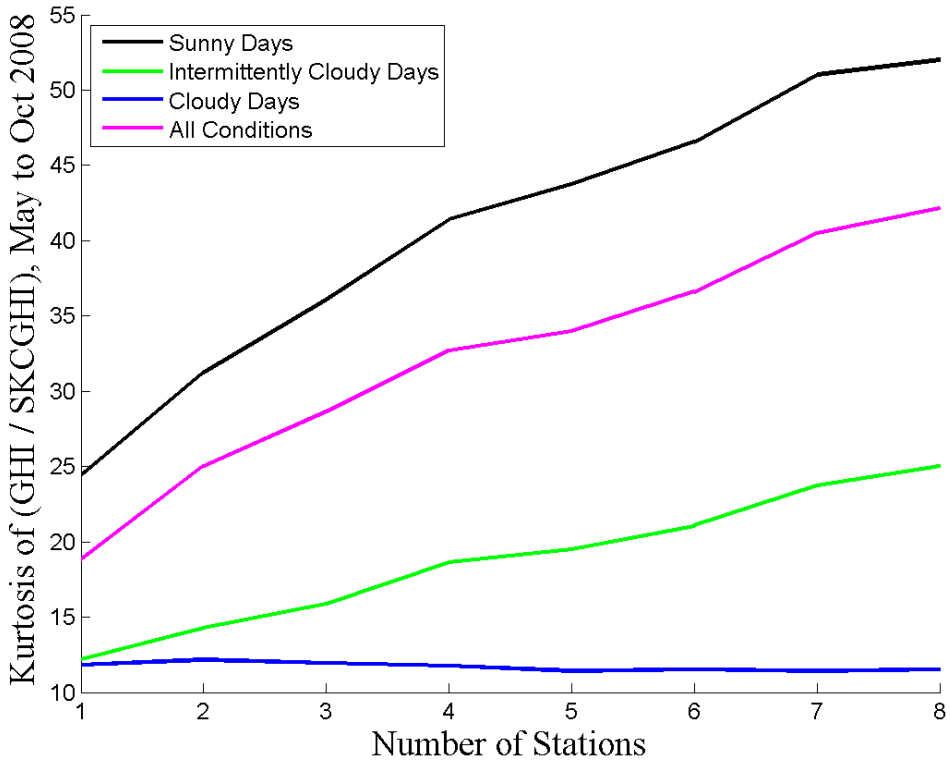


**Figure 23: Kurtosis of aggregate GHI RR at all sites from May to October 2008**

**Table 6: Statistical characteristics of aggregate RR, stratified by cloudiness for May through October 2008**

| | Ramp Rate Statistic | 1 Site | 2 Sites | 3 Sites | 4 Sites | 5 Sites | 6 Sites | 7 Sites | 8 Sites |
|---|---|---|---|---|---|---|---|---|---|
| **Any Cloudiness** | Variance ($min^{-2}*10^{-3}$) | 0.31 | 0.23 | 0.23 | 0.19 | 0.18 | 0.17 | 0.15 | 0.14 |
| | Kurtosis ($min^{-4}$) | 20.2 | 26.7 | 25.8 | 30.2 | 30.8 | 34.7 | 40.0 | 42.3 |
| **Sunny** | Variance ($min^{-2}*10^{-3}$) | 0.26 | 0.20 | 0.20 | 0.16 | 0.15 | 0.14 | 0.13 | 0.12 |
| | Kurtosis ($min^{-4}$) | 25.0 | 31.2 | 31.2 | 36.5 | 38.5 | 42.8 | 49.3 | 52.0 |
| **Intermittently Cloudy** | Variance ($min^{-2}*10^{-3}$) | 0.34 | 0.23 | 0.24 | 0.18 | 0.18 | 0.16 | 0.14 | 0.13 |
| | Kurtosis ($min^{-4}$) | 14.0 | 15.9 | 15.1 | 18.2 | 18.1 | 20.1 | 23.4 | 24.9 |
| **Cloudy** | Variance ($min^{-2}*10^{-3}$) | 0.36 | 0.24 | 0.26 | 0.23 | 0.24 | 0.23 | 0.22 | 0.21 |
| | Kurtosis ($min^{-4}$) | 10.7 | 12.0 | 11.3 | 10.8 | 10.4 | 10.9 | 11.1 | 11.5 |

# 4. DISCUSSION AND CONCLUSIONS

Certain meteorological phenomena are particularly pronounced in coastal environments. In San Diego summers, morning clouds frequently occlude the sky, which affects the measured GHI near to the ocean. As can be seen in the map of the sites in Figure 1, the Hubbs site is on the shoreline. The remainder of the sites is significantly more inland. This fact accounts for many of the results in this project.

The effect of the proximity to the ocean of the Hubbs site is exemplified in the one-to-one comparisons of GHI, where GHI at the Hubbs site is shown to be generally lower than at the other sites. Additionally, correlation coefficient analysis shows that GHI varies more greatly between sites as the distance between the sites is increased. Thus, based on these two analyses, it can be stated that GHI is generally lower nearer to the ocean and increases as the distance from the ocean is increased.

However, aside from characterizing the weather in this geographic region using GHI measurements and comparing site characteristics in relation to ocean proximity, this project aims to characterize the GHI seen by a distributed array of solar power sites and attempt to describe the power output from it.

It is reasonable to assume that net power output from an array of solar power sites is directly proportional to the incident GHI seen by the solar panels in said array. Thus, the measured GHI of this project can be used as a corollary for power output from the distributed array of interest. The analysis that yields the most insight into the net power output from a distributed array of solar sites is the aggregate RR and SS analysis.

It has been shown that the RR and SS of the aggregate GHI decreases significantly as more sites are added to the aggregate. This result implies that as a

distributed array is populated with more and more sites, the net power RR will decrease significantly. In other words, a larger distributed array will have a less variable power output.

Additionally, using this relationship of increasing array size to decreasing high net power RR, it can be hypothesized that the solar character of a given area, whether a suburban town, a densely packed city or a barren desert, could be quickly determined using a few solar "modeling" sites that were strategically positioned around the area of interest, accounting for geography, microclimates and other phenomena. The gathered GHI data could then be used to model the character of the net power produced for a distributed array of solar sites of a specified size in that region.

The results of the statistical analysis of the aggregate GHI RR are also particularly of interest to this project. As discussed, the variance of aggregate GHI RR deviating from SKCGHI on days with any cloudiness is shown to decrease as more sites are added to the aggregate. This result describes the averaging effect that a larger number of sites can produce. For example, if a few sites out of a hundred were covered by a cloud for a few minutes, the overall power output from the array would not be greatly diminished. However, if a few sites out of five were covered, the effect would be much more noticeable and RR would be higher.

However, more importantly, this decrease in variance with increase in site number describes a unique advantage to distributed arrays as compared to tightly packed arrays, which are typical of those in remote desert areas, termed solar farms. For example, if a cloud of a specified size were to drift across a distributed array, it may only occlude a few sites in the array at once and perhaps even none of the sites, depending on the size and path of the cloud and the layout of the array, resulting in

low net RR. Conversely, if this same cloud were to pass over a tightly packed array or solar farm, a much higher percentage of the array's solar sites would be obscured by the cloud, significantly increasing net RR[2]. Additionally, the cloud would continuously cover sites in the area until the cloud had exited the area completely, reducing overall power output by a much larger fraction than in a distributed array.

What this somewhat idealized example illustrates is the inherent capability of distributed solar arrays to reduce net RR given any cloudiness. The breadth of the area spanned by the sites allows different microclimates to be experienced simultaneously. This characteristic of distributed arrays is shown in this project's results (Figures 21b,d), where net RR is more greatly reduced on cloudier days than on sunnier days. Additionally, the spacing between the sites allows clouds to be present over the area without a significant reduction in net power output.

Also, the kurtosis on sunny days was shown to increase significantly with an increase in the number of sites in the array, while cloudy days exhibit no change in kurtosis. When this relationship is considered in combination with the decreasing of variance as the number of sites in the array increases, it can be concluded that, although more large disturbances are experienced by the array as a whole, the capability of distributed arrays to effectively absorb changes in GHI readily without large net RR allows a net power production nearer to SKC than that from an array with fewer or more tightly packed sites.

Overall, these conclusions show that increasing the population and area covered by a distributed array of solar sites serves to reduce its net power RR and decrease its susceptibility to microclimate weather variations. This conclusion could

[2] This situation would also increase variance. However, an analysis that compares distributed arrays to tightly packed arrays would need to be completed to verify this assertion.

therefore be expanded to consider a city-, county-, state- or even country-wide distributed solar array, most likely present on the roofs of residential homes.

Any array of this breadth and magnitude would adhere to the conclusions reached in this project. However, this isn't to say that a very large distributed array would be immune to all weather effects. Its power output would still ebb with widespread cloud cover and grow with clearer skies. However, because these changes in net power output are directly linked to GHI in a certain area, weather forecasting could be used to predict the power generated in a given area for a future time frame as distant as weather forecasting can be trusted to be accurate.

In summary, the GHI of a distributed array of 8 solar sites has been analyzed to produce a few simple yet reliable characteristics of a general distributed solar array. It is hoped that these characteristics will help to further incorporation of residential solar power throughout the state of California and beyond. Additionally, this project's stratification of days by cloudiness will hopefully inspire other researchers to use a similar technique to compare results of similar analyses with forecasted weather and yield information about what to expect for a future day with a given forecasted cloudiness.

To extend this project, power spectra of the measured GHI should be calculated and compared to further understand the intricacies of the intermittencies of the power produced. Additionally, a new form of analysis, called cospectral analysis, which has not been used in any literature to analyze GHI, should be used to further characterize the production of solar power at different frequencies.

# BIBLIOGRAPHY


1. **Luque, Antonio and Hegedus, Steven.** *Handbook of Photovoltaic Science and Engineering.* New York : John Wiley and Sons, 2003. ISBN 0471491969.

2. **Aabakken, J.** *Power Technologies Energy Data Book.* 4th. Golden : NREL: National Renewable Energies Laboratory, 2006. NREL/TP-620-39728.

3. *The Character of Power Output from Utility-Scale Photovoltaic Systems.* **Curtright, Aimee E. and Apt, Jay.** Pittsburgh : Wiley InterScience, 2007, Progress in Photovoltaics: Research and Applications, Vol. 16, pp. 241-247.

4. *Surface Measurements of Solar Irradiance: A Study of the Spatial Correlation between Simultaneous Measurements at Separated Sites.* **Long, Charles N. and Ackerman, Thomas P.** University Park : American Meteorological Society, May 1995.

5. *Wind Power Plant Behaviors: Analyses of Long-Term Wind Power Data.* **Wan, Yih-Huei.** Golden : NREL: National Renewable Energies Laboratory, September 2004. NREL/TP-500-36551.

6. *Voltage Fluctuations on Distribution Level Introduced by Photovoltaic Systems.* **Woyte, Achim.** 1, s.l. : IEEE, March 2006, IEEE Transactions on Energy Conservation, Vol. 21.

7. *Identification of clear skies from broadband pyranometer measurements and calculation of downwelling shortwave cloud effects.* **Long, Charles M. and Ackerman, Thomas P.** D12, University Park : Journal of Geophysical Research, June 27, 2000, Vol. 105, pp. 15,609-15,626.

8. **Chambers, Dr. Lin.** *My NASA Data Homepage.* [Online] s.l. : NASA, 2009.

9. **Gonzales, Chris and Wilcox, Steve.** *Sunny Days User's Manual.* [Microsoft Word Document] s.l. : National Renewable Energy Laboratory (NREL), 2004.

10. **Lee, C. C.** *Environmental Engineering Dictionary, 4th Edition.* New York : Rowman & Littlefield, 2005. ISBN 086587848X, 9780865878488.

11. **Ramana, B. V.** *Higher Engineering Mathematics.* New York : Tata McGraw-Hill, 2007. ISBN 007063419X, 9780070634190.

12. *The spectrum of power from wind turbines.* **Apt, Jay.** 2007, Journal of Power Sources, Vol. 169, pp. 369-374.

# APPENDIX

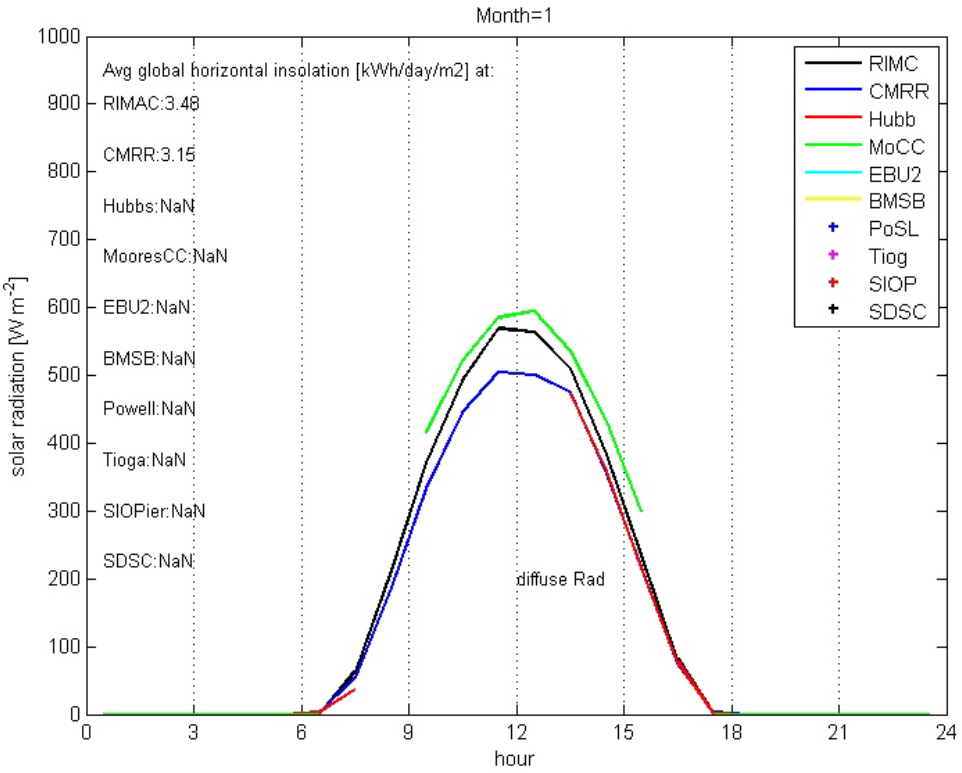


**Figure 10b: Average hourly solar irradiation flux by hour in January 2008**

c)

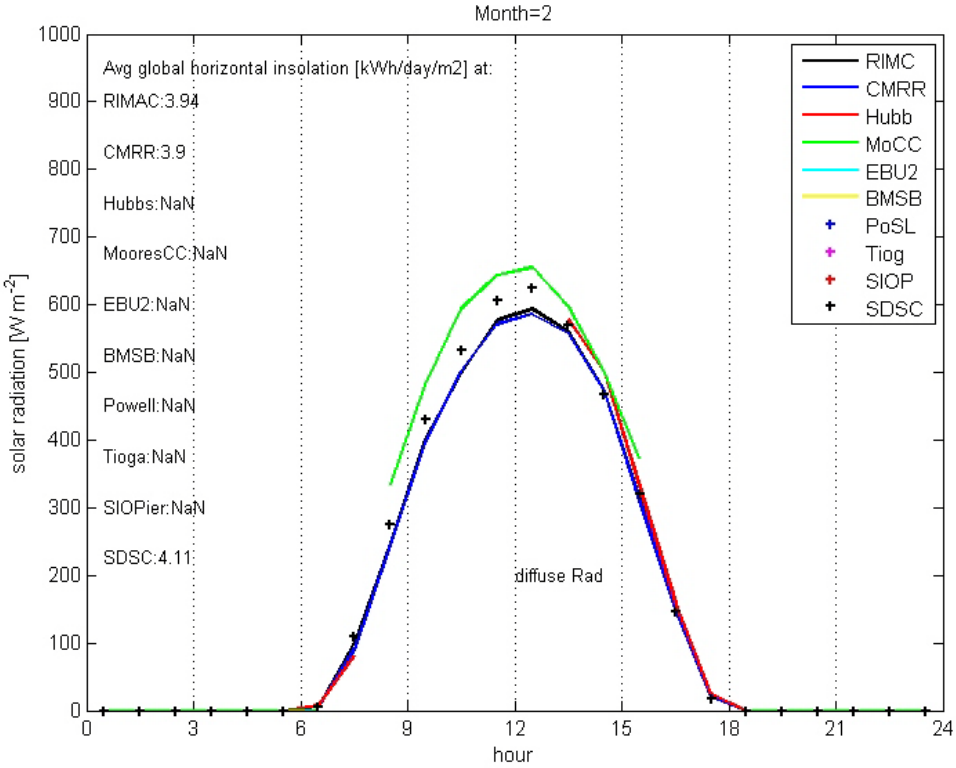


d)

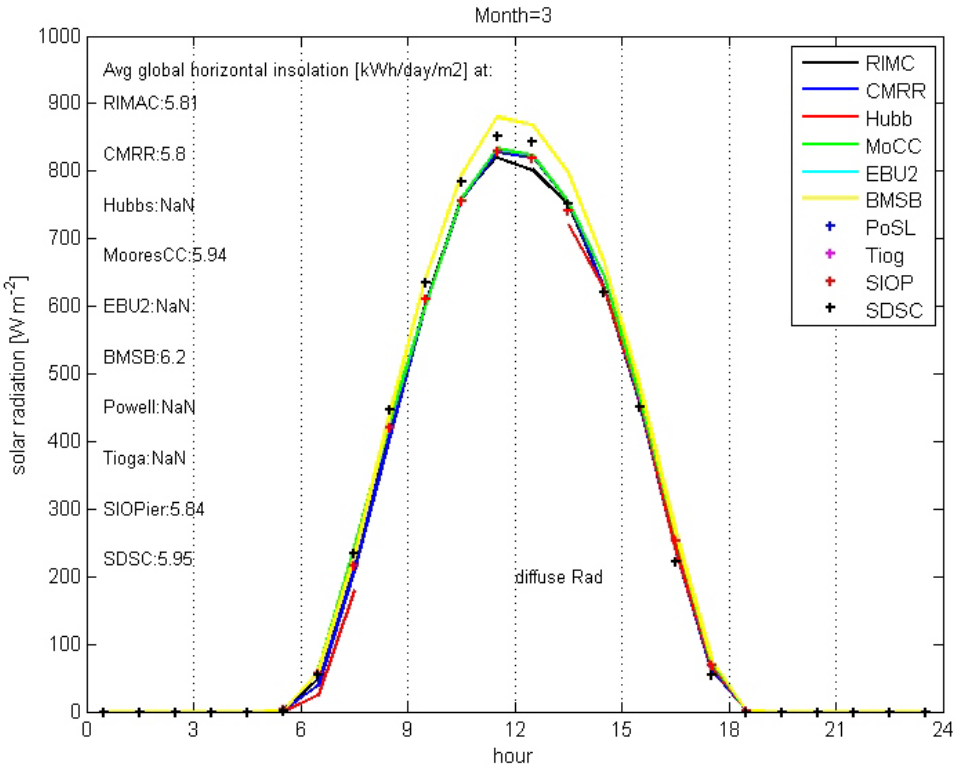


**Figure 10c,d: Average hourly solar irradiation flux by hour in: b) February; and c) March 2008**

e)

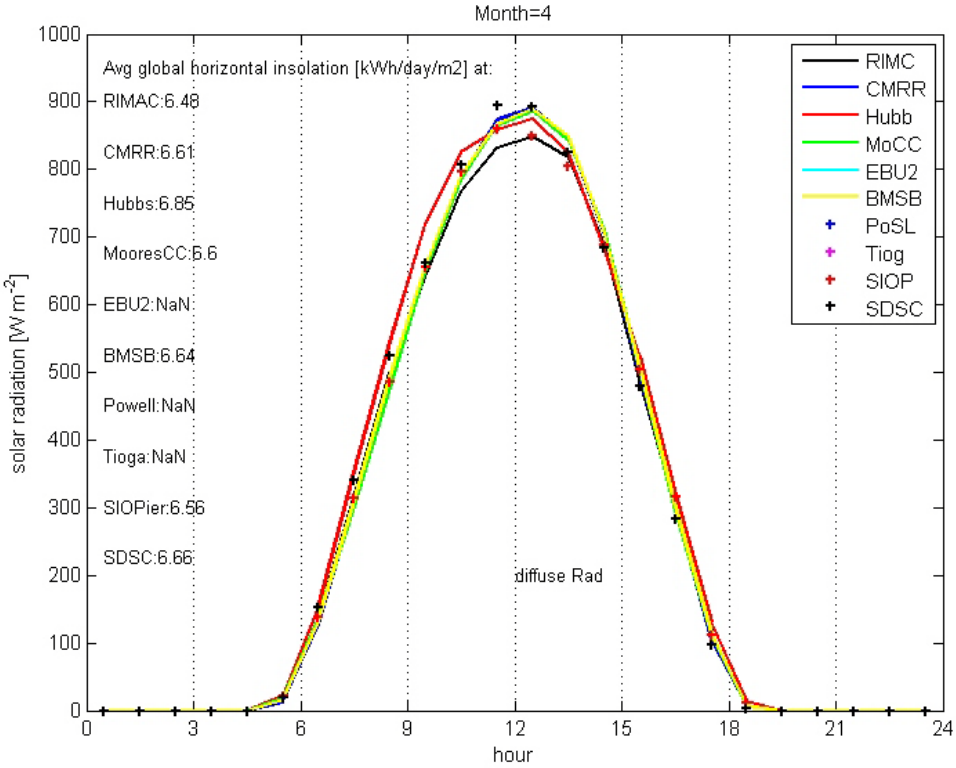


f)

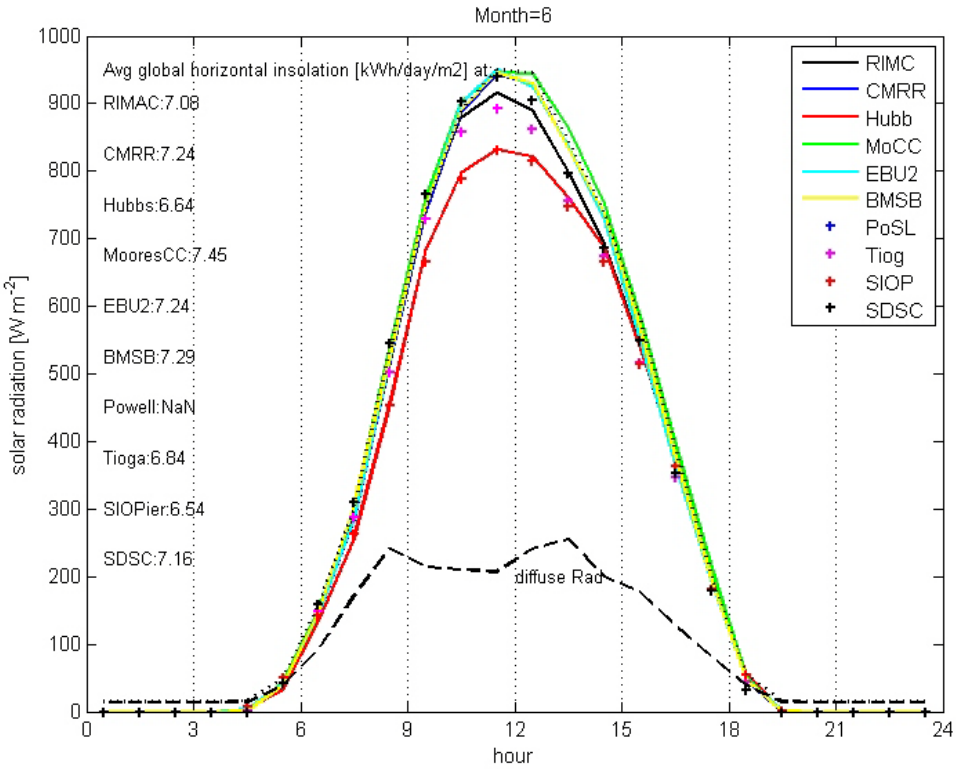


**Figure 10e,f: Average hourly solar irradiation flux by hour in: e) April; and f) June 2008**

g)

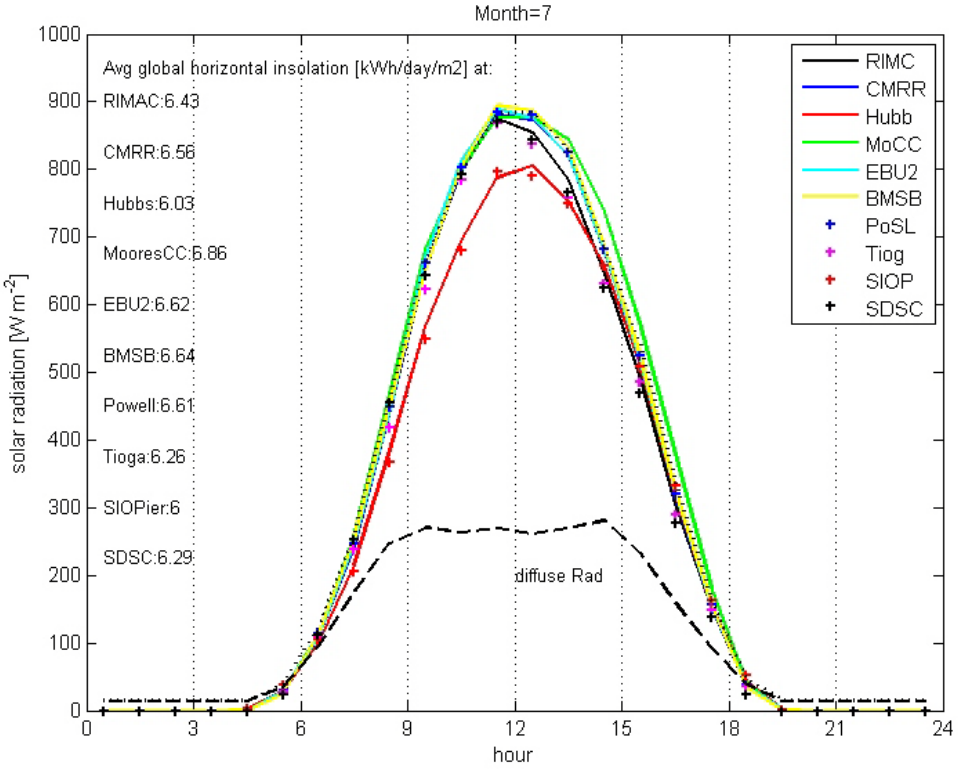


h)

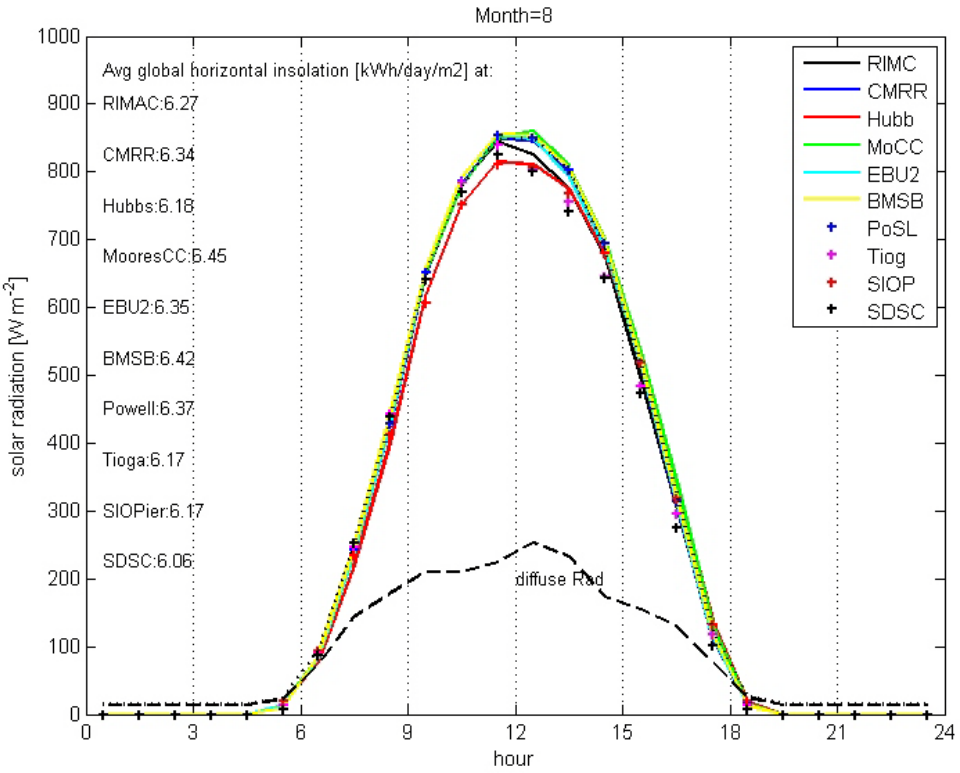


**Figure 10g,h: Average hourly solar irradiation flux by hour in: g) July; and h) August 2008**

i)

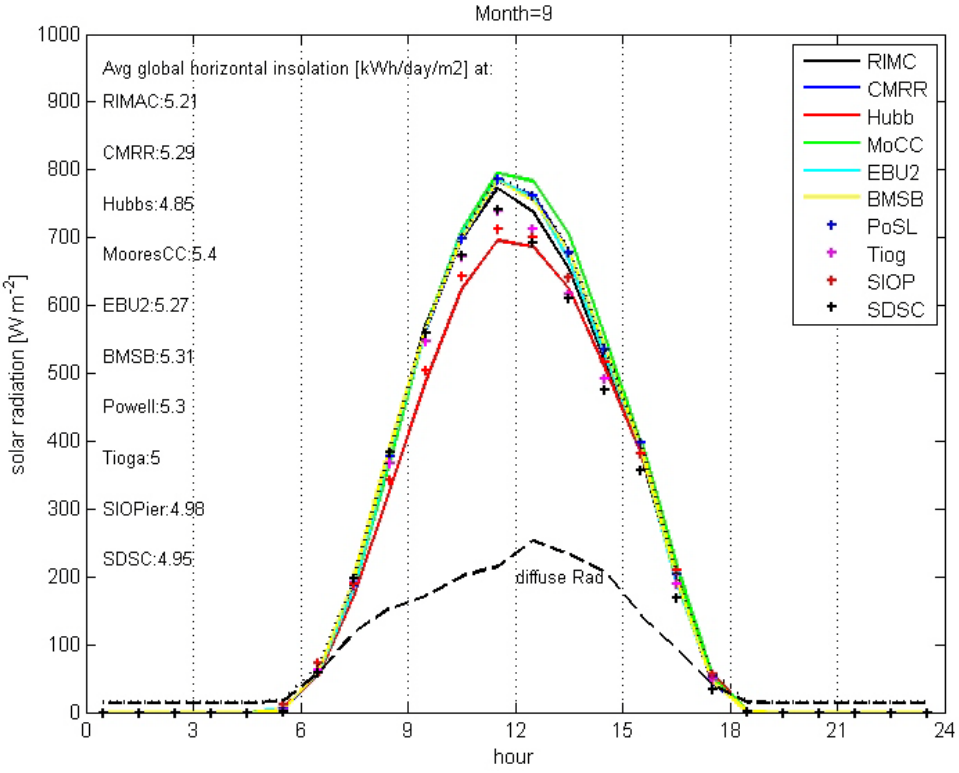


j)

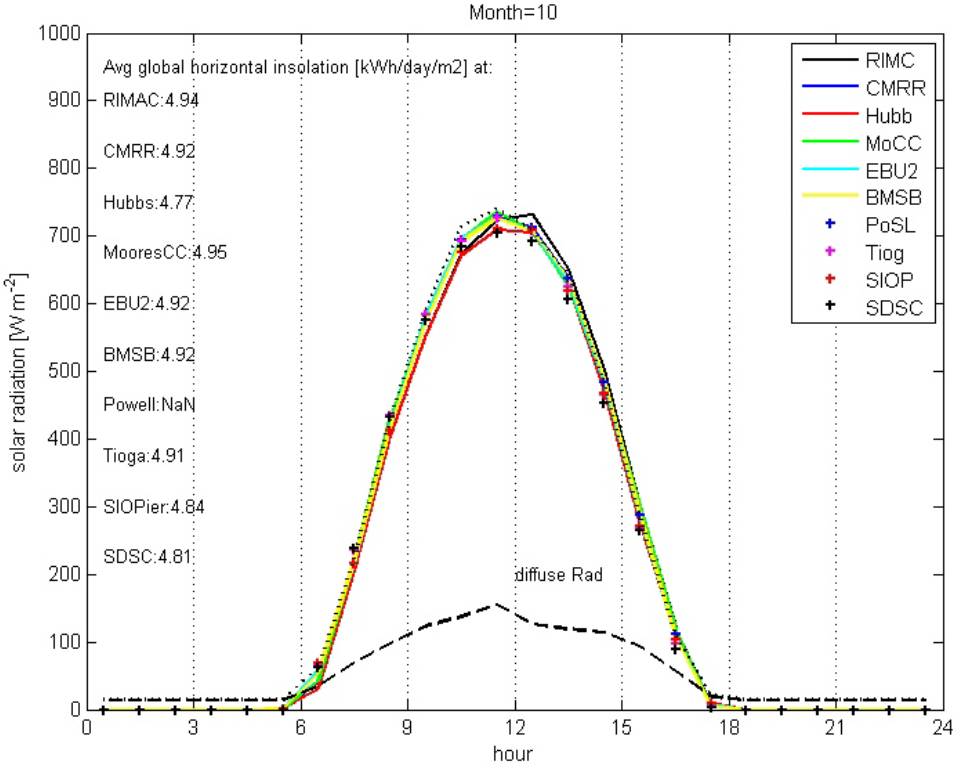


**Figure 10i,j: Average hourly solar irradiation flux by hour in: i) September; and j) October 2008**

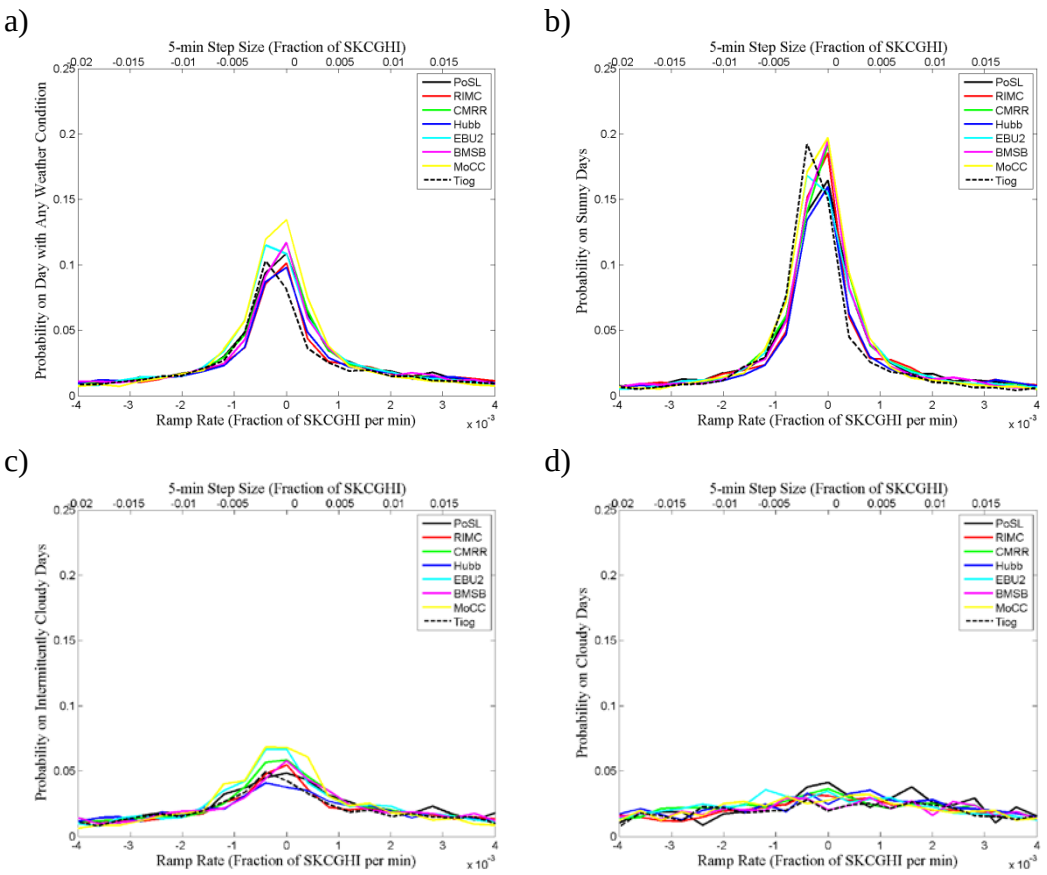


**Figure 18a-d: GHI RR and SS PDFs from May through July 2008 for days stratified as: a) any cloudiness; b) sunny; c) intermittently cloudy; and d) cloudy**

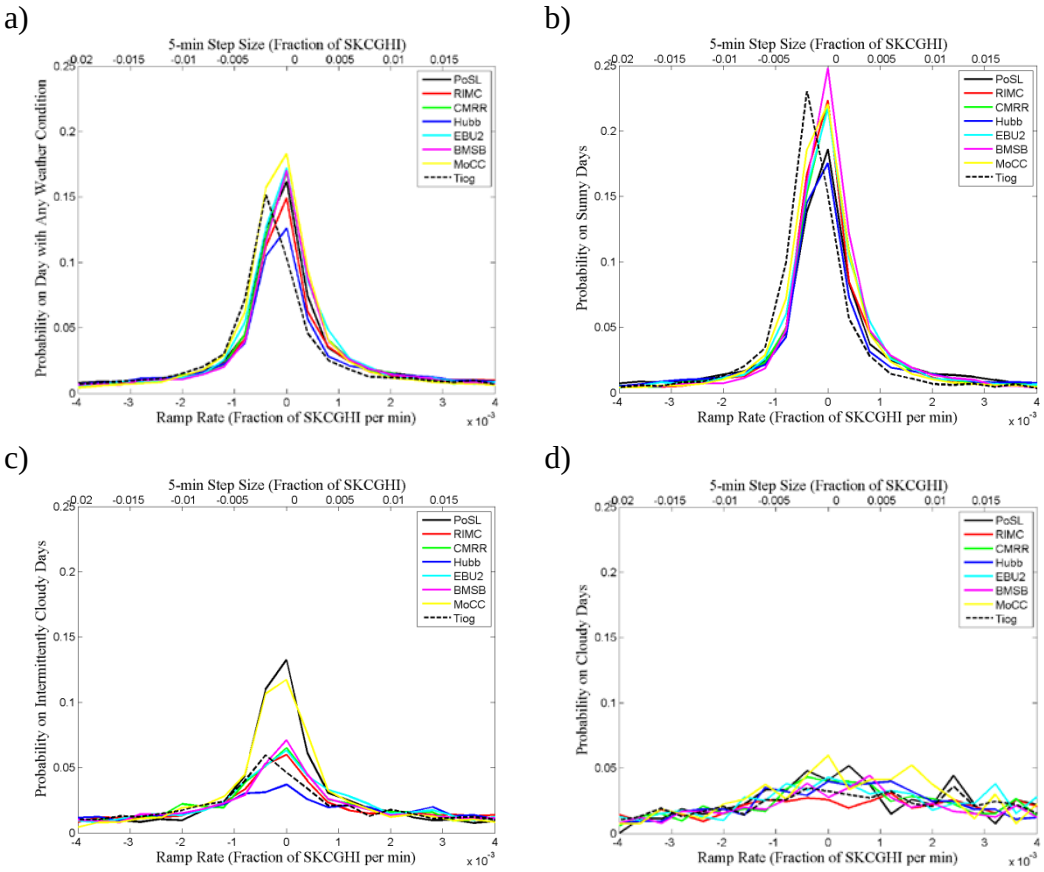


**Figure 19a-d: GHI RR and SS PDFs from August through October 2008 for days stratified as: a) any cloudiness; b) sunny; c) intermittently cloudy; and d) cloudy**